CR-124,045

RADIATION FROM SLOTTED-CYLINDER ANTENNAS, COATED WITH CONCENTRIC LAYERS OF DIELECTRIC MATERIAL

APR 1971
RECEIVED
NASA STI FACILITY
INPUT BRANCH

By

Calvin T. Swift

Thesis submitted to the Graduate Faculty of the
Virginia Polytechnic Institute
in candidacy for the degree of

MASTER OF SCIENCE

in

PHYSICS

April 1965

FACILITY FORM 602
N71 72377 (ACCESSION NUMBER) (THRU)
72 (PAGES) None (CODE)
TMX 67032 (NASA CR OR TMX OR AD NUMBER) (CATEGORY)

RADIATION FROM SLOTTED-CYLINDER ANTENNAS, COATED WITH CONCENTRIC LAYERS OF DIELECTRIC MATERIAL

By

Calvin T. Swift

ABSTRACT

A slotted-cylinder antenna, coated with concentric layers of conductive dielectric material is developed as a boundary value problem. The formalism follows the procedure as originally outlined by J. R. Wait, except that the boundary conditions are stated in matrix form. The problem is formulated so that the transforms of the four unknown tangential fields E_z, E_ϕ, H_z, and H_ϕ at the aperture are directly related to the two unknown vector potentials A_z and A_z through computable products of four-by-four matrices. Further information is then achieved by completing the boundary conditions at the aperture and algebraically solving for all unknowns.

As a means to check the procedure, the radiation fields of half-wave axial and circumferential aperture antennas, with specified electric field distributions, are computed and checked against known results.

RADIATION FROM SLOTTED-CYLINDER ANTENNAS, COATED WITH CONCENTRIC LAYERS OF DIELECTRIC MATERIAL

by

Calvin T. Swift

Thesis submitted to the Graduate Faculty of the
Virginia Polytechnic Institute
in candidacy for the degree of
MASTER OF SCIENCE
in
PHYSICS

April 1963

Blacksburg, Virginia

II. TABLE OF CONTENTS

III. LIST OF FIGURES AND TABLES

TABLES PAGE

IV. INTRODUCTION

When a high speed missile enters the atmosphere, air in the immediate vicinity heats up and produces free electrons. As the vehicle descends, the concentration of electrons may increase to such a degree that communications are interrupted. This "blackout" may persist for a considerable length of time, causing several problems in connection with space and defense missions. For example, additional provisions must be made for data storage; the plasma may interfere with ICBM homing devices; and information regarding catastrophic failures during blackout may be lost. For these reasons, and others, a continuing effort has been directed toward the theoretical analysis and possible alleviation of the problem.

The present effort is concerned with the theory, and as in most mathematical developments, certain simplifications are assumed. The model considered here is the infinitely long dielectric coated conducting cylinder, onto which is cut a radiating aperture. Although this is an idealized model, there are many features common between a reentry vehicle and the geometrical simplication. For instance, flush mounted aperture antennas are usually used to minimize aerodynamic drag; the aft portion of many reentry vehicles are cylindrical; and the plasma sheath existing between the body and the shock wave is a conductive dielectric.

The exterior theory of the slotted-cylinder antenna, coated with a homogeneous dielectric, was developed a few years ago by J. R. Wait (ref. 1). He approached the problem by expressing all fields in terms of Fourier transforms and then applying the boundary conditions to solve for all unknown coefficients. The radiation fields were found by evaluating the inverse transform by means of the saddle point method.

Wait's theory included a method of computing the far fields at a general point in space; however, graphical results were confined to the equatorial plane of a tangentially excited (axial) slot antenna. This restriction allowed mathematical simplifications which significantly reduced the computational labor.

Since Wait's original work, others have examined the problem in an effort to extend the results. Using an approach, essentially equivalent to Wait's, C. M. Knop (ref. 2) derived the far fields of an axially polarized (circumferential) slot. Although explicit far field expressions were given, Knop's results were also confined to the equatorial plane.

Following the suggestion in reference 1 (pp. 133-135), W. V. T. Rusch (ref. 3) simplified the problem somewhat by expressing the dielectric solutions in terms of a Taylor series expansion. It is noteworthy to remark that Rusch computed radiation patterns off the equatorial plane. However, only the first two terms of the series expansion were retained, indicating that his procedure fails if the product of the dielectric thickness times the radial wave number is large.

Recently, Meltz (ref. 4) computed equatorial patterns of the axial slot and elevation patterns of the circumferential gap antenna. By means of a computer subroutine giving Bessel functions of complex arguments, Meltz was able to explore the effects of loss in the dielectric coating.

Flow field analysis shows that the dielectric properties of the plasma may vary considerably, particularly in the radial direction; therefore, a further refinement in the propagation model can be made if the inhomogeniety is considered. In a previous paper by C. T. Swift (ref. 5), equatorial patterns of an infinitely long axial slot, covered with a radially varying plasma were calculated by directly integrating the wave equation. However, this procedure cannot easily be applied if the aperture is finite (see ref. 6 for an explanation). Instead, the inhomogeneous plasma will be replaced by several homogeneous tandem layers, judiciously chosen to fit the given distribution.

The problem was originally investigated by J. H. Harris (ref. 7), who devised a systematic procedure of expressing the free-space solutions in terms of the electric fields on the aperture. His data consisted of elevation patterns of an axial slot, coated with two dissimilar dielectrics.

The present effort extends the work of reference 7. A method is developed whereby the boundary conditions at each interface are expressed in terms of a 4×4 matrix. The $n + 1$ matrices, where n is the number of layers, are then systematically multiplied together.

Regardless of the number of layers, repetitive multiplication gives a single 4×4 matrix which relates all four of the tangential aperture fields to the two free-space coefficients. Additional information is then provided by completing the boundary conditions at the aperture.

As special cases, the far fields of half-wave axial and circumferential slots, with specified electric field excitations are computed; and the data are compared with results published elsewhere.

V. LIST OF SYMBOLS

$\vec{A}$	electric vector potential, volts/meter/sec
$\vec{A}^*$	magnetic vector potential, ampere-turns/meter/sec
a	radius of conducting cylinder, meters
$a\phi_o$	slot dimension in azimuthal direction, meters
$\vec{B}$	magnetic flux density, webers/square meter
b	radial distance to dielectric-air interface
$\vec{D}$	electric displacement, coulombs/square meter
$\vec{E}$	electric field intensity, volts/meter
$F_m(k_z)$	transform of electric vector potential, volts/sec
$G_m(k_z)$	transform of magnetic vector potential, ampere-turns/sec
$\vec{H}$	magnetic field intensity, ampere-turns/meter
$H_m^{(2)}(x)$	Hankel function of order m and argument x
$J_m(x)$	Bessel function of order m and argument x
J	$\sqrt{-1}$
k	wave number $= 2\pi/\lambda$, meters^{-1}
k_z	axial mode number, meters^{-1}
m	azimuthal mode number
$N_1\left(\frac{\pi}{2}, \phi\right)$	pattern normalization $\left[\frac{P_1\left(\frac{\pi}{2}, \phi\right)}{P_1\left(\frac{\pi}{2}, 0\right)}\right]^{1/2}$ for the axial slot

$N_2\left(\frac{\pi}{2}, \phi\right)$ pattern normalisation, $\left[\frac{P_2\left(\frac{\pi}{2}, \phi\right)}{P_2\left(\frac{\pi}{2}, 0\right)}\right]^{1/2}$ for the circumferential slot

N_e electron density, cm^{-3}

n index of refraction

$P_1\ (\theta, \phi)$ pattern factor for axial slot

$P_2\ (\theta, \phi)$ pattern factor for circumferential slot

r, θ, ϕ spherical coordinates

$\vec{S}$ real part of Poynting vector, watts/square meter

u radial mode number, $meters^{-1} = \sqrt{k^2 - k_z^2}$

$\vec{u}_z$ unit vector in axial direction

$\vec{u}_r$ unit vector in radial direction

V_o applied potential on slot, volts

x, y, z Cartesian coordinates

Z_o intrinsic impedance of free-space = 376.7 ohms

z_o slot dimension in axial direction, meters

δ_o^m Kronecker delta, $\begin{cases} = 1 & m = 0 \\ = 0 & m \neq 0 \end{cases}$

ϵ permittivity, farads/meter

λ wavelength, meters

μ_o permeability of free-space = $4\pi \times 10^{-7}$ henrys/meter

ν collision frequency, collisions/sec

ρ, ϕ, z cylindrical coordinates

Ψ electric scalar potential, volts

Ψ^* magnetic scalar potential, ampere-turns

ω frequency of propagation, radians/sec

ω_p plasma frequency = $2\pi \times 8.97 \times 10^3 \sqrt{N_e}$, radians/sec

Subscripts

o free-space value

i value in the ith dielectric layer

n value in last dielectric layer

r, θ, ϕ vector components in spherical coordinates

ρ, ϕ, z vector components in cylindrical coordinates

Superscripts

i vectors and matrices in ith dielectric layer

n vectors and matrices in last dielectric layer

n+1 vectors and matrices in free-space

A prime on the various Bessel functions denotes differentiation with respect to the argument

VI. THEORY

Development of the Exterior Problem in Matrix Form

The geometry is shown in figure 1. A radiating aperture antenna, of arbitrary shape and arbitrary spatial excitation, is cut into a long conducting cylinder which is coated with concentric layers of lossy dielectric. The fields within each layer, the ith for example, are derived from a pair of axial vector potentials, $A_z^i \vec{u}_z$ and $A_z^{i*} \vec{u}_z$, defined by

$$\left.\begin{aligned} \vec{B}^i &= \nabla \times A_z^i \vec{u}_z \\ \vec{D}^i &= -\nabla \times A_z^{i*} \vec{u}_z \end{aligned}\right\} \tag{1}$$

Physically, A_z^i describes TM (transverse magnetic to z) fields and A_z^{i*} describes TE (transverse electric to z) fields. These partial fields are then superimposed, assuming a temporal variation $e^{j\omega t}$, to give: (See appendix A.)

$$\left.\begin{aligned} \vec{E}^i &= \frac{1}{j\omega\mu_o \epsilon_i} \nabla \times \nabla \times A_z^i \vec{u}_z - \frac{1}{\epsilon_i} \nabla \times A_z^{i*} \vec{u}_z \\ \vec{H}^i &= \frac{1}{\mu_o} \nabla \times A_z^i \vec{u}_z + \frac{1}{j\omega\mu_o \epsilon_i} \nabla \times \nabla \times A_z^{i*} \vec{u}_z \end{aligned}\right\} \tag{2}$$

A_z^i and A_z^{i*} are solutions of the wave equation in cylindrical coordinates; that is

$$\left.\begin{aligned} A_z^i(\rho, \phi, z) &= \int_{-\infty}^{\infty} \sum_{m=-\infty}^{\infty} F_m^i(\rho, k_z) e^{-jm\phi} e^{-jk_z z} \, dk_z \\ A_z^{i*}(\rho, \phi, z) &= \int_{-\infty}^{\infty} \sum_{m=-\infty}^{\infty} G_m^i(\rho, k_z) e^{-jm\phi} e^{-jk_z z} \, dk_z \end{aligned}\right\} \quad (3)$$

where $F_m^i(\rho, k_z)$ and $G_m^i(\rho, k_z)$ are linear combinations of Bessel functions. In free-space $(i = n + 1)$, only outgoing wave exist, therefore

$$\left.\begin{aligned} F_m^{n+1}(\rho, k_z) &= c_m H_m^{(2)}(u_o \rho) \\ G_m^{n+1}(\rho, k_z) &= d_m H_m^{(2)}(u_o \rho) \end{aligned}\right\} \quad (4)$$

Each of the dielectric layers, the ith layer for instance, supports standing waves, therefore, $F_m^i(\rho, k_z)$ and $G_m^i(\rho, k_z)$ assume the form

$$\left.\begin{aligned} F_m^i(\rho, k_z) &= a_m^i J_m(u_i \rho) + A_m^i H_m^{(2)}(u_i \rho) \\ G_m^i(\rho, k_z) &= b_m^i J_m(u_i \rho) + B_m^i H_m^{(2)}(u_i \rho) \end{aligned}\right\} \quad (5)$$

for $i = 1, 2, \ldots, n$.

The unknown coefficients are specified by requiring continuity of the tangential components of $\vec{E}$ and $\vec{H}$ at the interface between each layer. From the schematic shown in figure 2, these boundary conditions are

$$E_{\phi}^{i}(\rho_{i+1}, \phi, z) = E_{\phi}^{i+1}(\rho_{i+1}, \phi, z)$$

$$E_{z}^{i}(\rho_{i+1}, \phi, z) = E_{z}^{i+1}(\rho_{i+1}, \phi, z) \qquad (6)$$

$$H_{\phi}^{i}(\rho_{i+1}, \phi, z) = H_{\phi}^{i+1}(\rho_{i+1}, \phi, z)$$

$$H_{z}^{i}(\rho_{i+1}, \phi, z) = H_{z}^{i+1}(\rho_{i+1}, \phi, z)$$

where $i = 1, 2, \ldots, n$. The substitution of equation (A-16) into equation (6) gives:

$$-\frac{k_z\, mF_m^i(k_z, \rho_{i+1})}{j\omega\mu_o\, \epsilon_i\, \rho_{i+1}} + \frac{1}{\epsilon_i}\frac{dG_m^i(k_z, \rho)}{d\rho}\bigg|_{\rho = \rho_{i+1}}$$

$$= -\frac{k_z\, mF_m^{i+1}(k_z, \rho_{i+1})}{j\omega\mu_o\, \epsilon_{i+1}\, \rho_{i+1}} + \frac{1}{\epsilon_{i+1}}\frac{dG_m^{i+1}(k_z, \rho)}{d\rho}\bigg|_{\rho = \rho_{i+1}}$$

$$\frac{u_i^2}{\epsilon_i} F_m^i(k_z, \rho_{i+1}) = \frac{u_{i+1}^2}{\epsilon_{i+1}} F_m^{i+1}(k_z, \rho_{i+1})$$

$$-\frac{k_z\, mG_m^i(k_z, \rho_{i+1})}{j\omega\mu_o\, \epsilon_i\, \rho_{i+1}} - \frac{1}{\mu_o}\frac{dF_m^i(k_z, \rho)}{d\rho}\bigg|_{\rho = \rho_{i+1}} \qquad (7)$$

$$= -\frac{k_z\, mG_m^{i+1}(k_z, \rho_{i+1})}{j\omega\mu_o\, \epsilon_{i+1}\, \rho_{i+1}} - \frac{1}{\mu_o}\frac{dF_m^{i+1}(k_z, \rho)}{d\rho}\bigg|_{\rho = \rho_{i+1}}$$

$$\frac{u_i^2}{\epsilon_i} G_m^i(k_z, \rho_{i+1}) = \frac{u_{i+1}^2}{\epsilon_{i+1}} G_m^{i+1}(k_z, \rho_{i+1})$$

where the azimuthal Fourier series, and the axial Fourier integral have been removed from the orthogonality relationships.

Equation (7) can be rearranged to give

$$
\left.
\begin{aligned}
F_m^i(k_z, \rho_{i+1}) &= \frac{\epsilon_i}{\epsilon_{i+1}} \frac{u_{i+1}^2}{u_i^2} F_m^{i+1}(k_z, \rho_{i+1}) \\
&\cdots\cdots \\
\left.\frac{dF_m^i(k_z, \rho)}{d\rho}\right|_{\rho=\rho_{i+1}} &= \left.\frac{dF_m^{i+1}(k_z, \rho)}{d\rho}\right|_{\rho=\rho_{i+1}} \\
&+ \frac{j\omega\mu_o m k_z}{u_i^2 \rho_{i+1}}\left(1 - \frac{\epsilon_i}{\epsilon_{i+1}}\right) G_m^{i+1}(k_z, \rho_{i+1}) \\
&\cdots\cdots \\
G_m^i(k_z, \rho_{i+1}) &= \frac{\epsilon_i}{\epsilon_{i+1}} \frac{u_{i+1}^2}{u_i^2} G_m^{i+1}(k_z, \rho_{i+1}) \\
&\cdots\cdots \\
\left.\frac{dG_m^i(k_z, \rho)}{d\rho}\right|_{\rho=\rho_{i+1}} &= \frac{\epsilon_i}{\epsilon_{i+1}}\left\{\left.\frac{dG_m^{i+1}(k_z, \rho)}{d\rho}\right|_{\rho=\rho_{i+1}}\right. \\
&\left. - \frac{j\omega\epsilon_{i+1} m k_z}{u_i^2 \rho_{i+1}}\left(1 - \frac{\epsilon_i}{\epsilon_{i+1}}\right) F_m^{i+1}(k_z, \rho_{i+1})\right\}
\end{aligned}
\right\} \quad (8)
$$

If equation (5) is subetituted into equation (8), then the boundary conditions, in matrix form, become

$$
A_{jk}^{i+1}\begin{Bmatrix} e_m^i \\ A_m^i \\ b_m^i \\ B_m^i \end{Bmatrix} = \left[B_{jk}^{i+1}\right]\begin{Bmatrix} e_m^{i+1} \\ A_m^{i+1} \\ b_m^{i+1} \\ B_m^{i+1} \end{Bmatrix} \quad (9)
$$

where

$$\left[A_{jk}^{\,i+1}\right] = \begin{bmatrix} J_m(u_i\rho_{i+1}) & H_m^{(2)}(u_i\rho_{i+1}) & 0 & 0 \\ u_i J_m'(u_i\rho_{i+1}) & u_i H_m^{(2)\prime}(u_i\rho_{i+1}) & 0 & 0 \\ 0 & 0 & J_m(u_i\rho_{i+1}) & H_m^{(2)}(u_i\rho_{i+1}) \\ 0 & 0 & u_i J_m'(u_i\rho_{i+1}) & u_i H_m^{(2)\prime}(u_i\rho_{i+1}) \end{bmatrix} \tag{10}$$

and

$$\left[B_{jk}^{\,i+1}\right] = \begin{bmatrix} \left(\frac{k_i u_{i+1}}{k_{i+1} u_i}\right)^2 J_m(u_{i+1}\rho_{i+1}) & \left(\frac{k_i u_{i+1}}{k_{i+1} u_i}\right)^2 H_m^{(2)}(u_{i+1}\rho_{i+1}) & 0 & 0 \\ u_{i+1} J_m'(u_{i+1}\rho_{i+1}) & u_{i+1} H_m^{(2)\prime}(u_{i+1}\rho_{i+1}) & \frac{j\omega\mu_o m k_z}{u_i^2 \rho_{i+1}}\left(1 - \frac{k_i^2}{k_{i+1}^2}\right) J_m(u_{i+1}\rho_{i+1}) & \frac{j\omega\mu_o m k_z}{u_i^2 \rho_{i+1}}\left(1 - \frac{k_i^2}{k_{i+1}^2}\right) H_m^{(2)}(u_{i+1}\rho_{i+1}) \\ 0 & 0 & \left(\frac{k_i u_{i+1}}{k_{i+1} u_i}\right)^2 J_m(u_{i+1}\rho_{i+1}) & \left(\frac{k_i u_{i+1}}{k_{i+1} u_i}\right)^2 H_m^{(2)}(u_{i+1}\rho_{i+1}) \\ \frac{j\omega\epsilon_o m k_z k_i^2}{k_o^2 u_i^2 \rho_{i+1}}\left(1 - \frac{k_i^2}{k_{i+1}^2}\right) J_m(u_{i+1}\rho_{i+1}) - \frac{j\omega\epsilon_o m k_z k_i^2}{k_o^2 u_i^2 \rho_{i+1}}\left(1 - \frac{k_i^2}{k_{i+1}^2}\right) H_m^{(2)}(u_{i+1}\rho_{i+1}) & u_{i+1}\left(\frac{k_i}{k_{i+1}}\right)^2 J_m'(u_{i+1}\rho_{i+1}) & u_{i+1}\left(\frac{k_i}{k_{i+1}}\right)^2 H_m^{(2)\prime}(u_{i+1}\rho_{i+1}) \end{bmatrix} \tag{11}$$

From the Wronskian relationship

$$J_m(u_i\rho_{i+1}) H_m^{(2)\prime}(u_i\rho_{i+1}) - H_m^{(2)}(u_i\rho_{i+1}) J_m'(u_i\rho_{i+1}) = -\frac{2_i}{\pi u_i \rho_{i+1}} \tag{12}$$

it follows that the inverse matrix, $\left[A_{jk}^{\,i+1}\right]^{-1}$ is

$$\left[A_{jk}^{\,i+1}\right]^{-1} = \begin{bmatrix} j\frac{\pi}{2}u_i\rho_{i+1}H_m^{(2)'}(u_i\rho_{i+1}) & -j\frac{\pi}{2}\rho_{i+1}H_m^{(2)}(u_i\rho_{i+1}) & 0 & 0 \\ -j\frac{\pi}{2}u_i\rho_{i+1}J_m'(u_i\rho_{i+1}) & j\frac{\pi}{2}\rho_{i+1}J_m(u_i\rho_{i+1}) & 0 & 0 \\ 0 & 0 & j\frac{\pi}{2}u_i\rho_{i+1}H_m^{(2)'}(u_i\rho_{i+1}) & -j\frac{\pi}{2}\rho_{i+1}H_m^{(2)}(u_i\rho_{i+1}) \\ 0 & 0 & -j\frac{\pi}{2}u_i\rho_{i+1}J_m'(u_i\rho_{i+1}) & j\frac{\pi}{2}\rho_{i+1}J_m(u_i\rho_{i+1}) \end{bmatrix} \tag{13}$$

Consequently, a new matrix $\left[C_{jk}^{\,i+1}\right] = \left[A_{jk}^{\,i+1}\right]^{-1}\left[B_{jk}^{\,i+1}\right]$ can be defined whose elements are

$$\left.\begin{aligned} C_{11}^{\,i+1} &= j\frac{\pi}{2}u_i\rho_{i+1}\left(\frac{k_iu_{i+1}}{k_{i+1}u_i}\right)^2H_m^{(2)'}(u_i\rho_{i+1})J_m(u_{i+1}\rho_{i+1}) - j\frac{\pi}{2}u_{i+1}\rho_{i+1}H_m^{(2)}(u_i\rho_{i+1})J_m'(u_{i+1}\rho_{i+1}) \\ C_{12}^{\,i+1} &= j\frac{\pi}{2}u_i\rho_{i+1}\left(\frac{k_iu_{i+1}}{k_{i+1}u_i}\right)^2H_m^{(2)'}(u_i\rho_{i+1})H_m^{(2)}(u_{i+1}\rho_{i+1}) - j\frac{\pi}{2}u_{i+1}\rho_{i+1}H_m^{(2)}(u_i\rho_{i+1})H_m^{(2)'}(u_{i+1}\rho_{i+1}) \\ C_{13}^{\,i+1} &= -j\frac{\pi}{2}\rho_{i+1}\left[\frac{j\omega\mu_o mk_z}{u_i^{\,2}\rho_{i+1}}\left(1-\frac{k_i^{\,2}}{k_{i+1}^{\,2}}\right)\right]H_m^{(2)}(u_i\rho_{i+1})J_m(u_{i+1}\rho_{i+1}) \end{aligned}\right\}$$

$$C_{14}^{i+1} = -j\frac{\pi}{2}\rho_{i+1}\left[\frac{j\omega\mu_o\, mk_z}{u_i^2\,\rho_{i+1}}\left(1-\frac{k_i^2}{k_{i+1}^2}\right)\right]H_m^{(2)}(u_i\rho_{i+1})H_m^{(2)}(u_{i+1}\rho_{i+1})$$

$$C_{21}^{i+1} = -j\frac{\pi}{2}u_i\rho_{i+1}\left(\frac{k_i\,u_{i+1}}{k_{i+1}\,u_i}\right)^2 J_m'(u_i\rho_{i+1})J_m(u_{i+1}\rho_{i+1}) + j\frac{\pi}{2}u_{i+1}\rho_{i+1}J_m(u_i\rho_{i+1})J_m'(u_{i+1}\rho_{i+1})$$

$$C_{22}^{i+1} = -j\frac{\pi}{2}u_1\rho_{i+1}\left(\frac{k_i\,u_{i+1}}{k_{i+1}\,u_i}\right)^2 J_m'(u_i\rho_{i+1})H_m^{(2)}(u_{i+1}\rho_{i+1}) + j\frac{\pi}{2}u_{i+1}\rho_{i+1}J_m(u_i\rho_{i+1})H_m^{(2)'}(u_{i+1}\rho_{i+1})$$

$$C_{23}^{i+1} = j\frac{\pi}{2}\rho_{i+1}\left[\frac{j\omega\mu_o\, mk_z}{u_i^2\,\rho_{i+1}}\left(1-\frac{k_i^2}{k_{i+1}^2}\right)\right]J_m(u_i\rho_{i+1})J_m(u_{i+1}\rho_{i+1})$$

$$C_{24}^{i+1} = j\frac{\pi}{2}\rho_{i+1}\left[\frac{j\omega\mu_o\, mk_z}{u_i^2\,\rho_{i+1}}\left(1-\frac{k_i^2}{k_{i+1}^2}\right)\right]J_m(u_i\rho_{i+1})H_m^{(2)}(u_{i+1}\rho_{i+1}) \qquad (14)$$

$$C_{31}^{i+1} = j\frac{\pi}{2}\rho_{i+1}\left[\frac{j\omega\epsilon_o\, mk_z\, k_i^2}{k_o^2\,u_i^2\,\rho_{i+1}}\left(1-\frac{k_i^2}{k_{i+1}^2}\right)\right]H_m^{(2)}(u_i\rho_{i+1})J_m(u_{i+1}\rho_{i+1})$$

$$C_{32}^{i+1} = j\frac{\pi}{2}\rho_{i+1}\left[\frac{j\omega\epsilon_o\, mk_z\, k_i^2}{k_o^2\,u_i^2\,\rho_{i+1}}\left(1-\frac{k_i^2}{k_{i+1}^2}\right)\right]H_m^{(2)}(u_i\rho_{i+1})H_m^{(2)}(u_{i+1}\rho_{i+1})$$

$$C_{33}^{i+1} = j\frac{\pi}{2}u_i\rho_{i+1}\left(\frac{k_i\,u_{i+1}}{k_{i+1}\,u_i}\right)^2 H_m^{(2)'}(u_i\rho_{i+1})J_m(u_{i+1}\rho_{i+1}) - j\frac{\pi}{2}u_{i+1}\rho_{i+1}\left(\frac{k_i}{k_{i+1}}\right)^2 H_m^{(2)}(u_i\rho_{i+1})J_m'(u_{i+1}\rho_{i+1})$$

$$C_{34}^{i+1} = j\frac{\pi}{2}u_i\rho_{i+1}\left(\frac{k_i u_{i+1}}{k_{i+1}u_i}\right)^2 H_m^{(2)\prime}(u_i\rho_{i+1})H_m^{(2)}(u_{i+1}\rho_{i+1}) - j\frac{\pi}{2}u_{i+1}\rho_{i+1}\left(\frac{k_i}{k_{i+1}}\right)^2 H_m^{(2)}(u_i\rho_{i+1})H_m^{(2)\prime}(u_{i+1}\rho_{i+1})$$

$$C_{41}^{i+1} = j\frac{\pi}{2}\rho_{i+1}\left[-\frac{j\omega\epsilon_o m k_z k_i^2}{k_o^2 u_i^2 \rho_{i+1}}\left(1 - \frac{k_i^2}{k_{i+1}^2}\right)\right]J_m(u_i\rho_{i+1})J_m(u_{i+1}\rho_{i+1})$$

$$C_{42}^{i+1} = j\frac{\pi}{2}\rho_{i+1}\left[-\frac{j\omega\epsilon_o m k_z k_i^2}{k_o^2 u_i^2 \rho_{i+1}}\left(1 - \frac{k_i^2}{k_{i+1}^2}\right)\right]J_m(u_i\rho_{i+1})H_m^{(2)}(u_{i+1}\rho_{i+1})$$

$$C_{43}^{i+1} = -j\frac{\pi}{2}u_i\rho_{i+1}\left(\frac{k_i u_{i+1}}{k_{i+1}u_i}\right)^2 J_m'(u_i\rho_{i+1})J_m(u_{i+1}\rho_{i+1}) + j\frac{\pi}{2}u_{i+1}\rho_{i+1}\left(\frac{k_i}{k_{i+1}}\right)^2 J_m(u_i\rho_{i+1})J_m'(u_{i+1}\rho_{i+1})$$

$$C_{44}^{i+1} = -j\frac{\pi}{2}u_i\rho_{i+1}\left(\frac{k_i u_{i+1}}{k_{i+1}u_i}\right)^2 J_m'(u_i\rho_{i+1})H_m^{(2)}(u_{i+1}\rho_{i+1}) + j\frac{\pi}{2}u_{i+1}\rho_{i+1}\left(\frac{k_i}{k_{i+1}}\right)^2 J_m(u_i\rho_{i+1})H_m^{(2)\prime}(u_{i+1}\rho_{i+1})$$

Therefore

$$\begin{Bmatrix} a_m^i \\ A_m^i \\ b_m^i \\ B_m^i \end{Bmatrix} = \left[C_{jk}^{i+1}\right] \begin{Bmatrix} a_m^{i+1} \\ A_m^{i+1} \\ b_m^{i+1} \\ B_m^{i+1} \end{Bmatrix} \qquad (15)$$

If i is replaced by i-1, the above equation becomes

$$\begin{Bmatrix} a_m^{i-1} \\ A_m^{i-1} \\ b_m^{i-1} \\ B_m^{i-1} \end{Bmatrix} = \left[C_{jk}^{i}\right] \begin{Bmatrix} a_m^{i} \\ A_m^{i} \\ b_m^{i} \\ B_m^{i} \end{Bmatrix} = \left[C_{jk}^{i}\right] \left[C_{jk}^{i+1}\right] \begin{Bmatrix} a_m^{i+1} \\ A_m^{i+1} \\ b_m^{i+1} \\ B_m^{i+1} \end{Bmatrix} \tag{16}$$

And, by repetition of the procedure given in equation (16) it follows that

$$\begin{Bmatrix} a_m^{1} \\ A_m^{1} \\ b_m^{1} \\ B_m^{1} \end{Bmatrix} = \left[C_{jk}^{2}\right]\left[C_{jk}^{3}\right] \cdots \left[C_{jk}^{n-1}\right]\left[C_{jk}^{n}\right] \begin{Bmatrix} a_m^{n} \\ A_m^{n} \\ b_m^{n} \\ B_m^{n} \end{Bmatrix} \tag{17}$$

Now, from equations (4), (5), and (8)

$$\left[A_{jk}^{n+1}\right] \begin{Bmatrix} a_m^{n} \\ A_m^{n} \\ b_m^{n} \\ B_m^{n} \end{Bmatrix} = \left[B_{jk}^{n+1}\right] \begin{Bmatrix} 0 \\ c_m \\ 0 \\ d_m \end{Bmatrix} \tag{18}$$

which implies that equation (17) becomes

$$\begin{Bmatrix} a_m^1 \\ A_m^1 \\ b_m^1 \\ B_m^1 \end{Bmatrix} = \left[C_{jk}^{\,2}\right]\left[C_{jk}^{\,3}\right]\cdots\left[C_{jk}^{\,n-1}\right]\left[C_{jk}^{\,n}\right]\left[C_{jk}^{\,n+1}\right] \begin{Bmatrix} 0 \\ c_m \\ 0 \\ d_m \end{Bmatrix} \tag{19}$$

When the boundary conditions are met at the ground plane, the coefficients a_m^1, A_m^1, b_m^1 and B_m^1 can be eliminated in favor of the modes of the trangential field components. To do this, the modes of the fields must be defined in terms of an azimuthal Fourier series and an axial Fourier integral. From Wait (ref. 1)

$$E_\phi(a, \phi, z) = \sum_{m=-\infty}^{\infty} e^{-jm\phi} \int_{-\infty}^{\infty} \bar{E}_{m\phi}(a, k_z)\, e^{-jk_z z}\, dk_z \tag{20}$$

where $\bar{E}_{m\phi}(a, k_z)$ is defined by the inverse transform

$$\bar{E}_{m\phi}(a, k_z) = \frac{1}{(2\pi)^2} \int_{-\pi}^{\pi} \int_{-\infty}^{\infty} E_\phi(a, \phi, z)\, e^{jm\phi}\, e^{jk_z z}\, d\phi\, dz \tag{21}$$

with $E_z(a, \phi, z)$, $H_\phi(a, \phi, z)$, and $H_z(a, \phi, z)$ similarly defined. Then, from equations (A-16)

$$\bar{E}_{m\phi}(a, k_z) = -\frac{k_z\, m k_o^2\, F_m^1(k_z, a)}{j\omega\mu_o\, \epsilon_o\, k_1^2\, a} + \left(\frac{k_o}{k_1}\right)^2 \frac{1}{\epsilon_o} \left.\frac{dG_m^1}{d\rho}\right|_{\rho=a} \tag{22}$$

$$\bar{E}_{mz}(a, k_z) = \left(\frac{u_1\, k_o}{k_1}\right)^2 \frac{F_m^1(k_z, a)}{j\omega\mu_o\, \epsilon_o}$$

$$\bar{H}_{m\phi}(a, k_z) = -\frac{k_z\, m k_o^2}{j\omega\mu_o\, \epsilon_o\, k_1^2\, a} G_m^1(k_z, a) - \frac{1}{\mu_o} \left.\frac{d}{d\rho} F_m^1(k_z, \rho)\right|_{\rho=a}$$

$$\bar{H}_{mz}(a, k_z) = \frac{u_1\, k_o}{k_1}^2 \frac{G_m^1(k_z, a)}{j\omega\mu_o\, \epsilon_o}$$

Equation (21), in matrix form is

$$\begin{Bmatrix} \bar{E}_{mz} \\ \bar{H}_{m\phi} \\ \bar{H}_{mz} \\ \bar{E}_{m\phi} \end{Bmatrix} = \left[D_{jk}^1\right] \begin{Bmatrix} a_m^1 \\ A_m^1 \\ b_m^1 \\ B_m^1 \end{Bmatrix} = \left[D_{jk}^1\right]\left[C_{jk}^2\right]\left[C_{jk}^3\right] \cdots \left[C_{jk}^n\right]\left[C_{jk}^{n+1}\right] \begin{Bmatrix} 0 \\ c_m \\ 0 \\ d_m \end{Bmatrix} \tag{23}$$

where

$$\left[D_{jk}^{1}\right] = \begin{bmatrix} \left(\frac{u_1 k_o}{k_1}\right)^2 \frac{J_m(u_1 a)}{j\omega\mu_o \epsilon_o} & \left(\frac{u_1 k_o}{k_1}\right)^2 \frac{H_m^{(2)}(u_1 a)}{j\omega\mu_o \epsilon_o} & 0 & 0 \\ -\frac{u_1}{\mu_o} J_m'(u_1 a) & -\frac{u_1}{\mu_o} H_m^{(2)'}(u_1 a) & -\frac{mk_z k_o^2 J_m(u_1 a)}{j\omega\mu_o \epsilon_o k_1^2 a} & -\frac{mk_z k_o^2}{j\omega\mu_o \epsilon_o k_1^2 a} H_m^{(2)}(u_1 a) \\ 0 & 0 & \left(\frac{u_1 k_o}{k_1}\right)^2 \frac{J_m(u_1 a)}{j\omega\mu_o \epsilon_o} & \left(\frac{u_1 k_o}{k_1}\right)^2 \frac{H_m^{(2)}(u_1 a)}{j\omega\mu_o \epsilon_o} \\ -\frac{k_z mk_o^2 J_m(u_1 a)}{j\omega\mu_o \epsilon_o k_1^2 a} & -\frac{k_z mk_o^2 H_m^{(2)}(u_1 a)}{j\omega\mu_o \epsilon_o k_1^2 a} & \left(\frac{k_o}{k_1}\right)^2 \frac{u_1}{\epsilon_o} J_m'(u_1 a) & \left(\frac{k_o}{k_1}\right)^2 \frac{u_1}{\epsilon_o} H_m^{(2)'}(u_1 a) \end{bmatrix} \tag{24}$$

For compactness of notation, the transformed fields at $\rho = a$ will be related to c_m and d_m through a single 4 by 4 matrix, that is,

$$\begin{Bmatrix} \bar{E}_{mz}(a, k_z) \\ \bar{H}_{m\phi}(a, k_z) \\ \bar{H}_{mz}(a, k_z) \\ \bar{E}_{m\phi}(a, k_z) \end{Bmatrix} = \left[L_{jk}(m, k_z)\right] \begin{Bmatrix} 0 \\ c_m(k_z) \\ 0 \\ d_m(k_z) \end{Bmatrix} \tag{25}$$

where $\left[L_{jk}\right]$ is the product of the matrices given in equation (23)

The Half-Wave Axial and Circumferential Slot Antennas

A complete solution of the problem requires a detailed study of the interior region of the cylinder ($\rho < a$). This treatment is possible. However, the boundary conditions are usually mixed and are therefore difficult to realize[1]. To avoid these complications, electric fields will be assumed on the slot, so that the coefficients, c_m and d_m, can be defined entirely by the transformed electric fields, $\bar{E}_{m\phi}(a, k_z)$ and $\bar{E}_{mz}(a, k_z)$, (ref. 1). If the electric field distribution is not altered by the coating, the following calculations will properly give the angular distribution of radiation, however, the prediction of the magnitude requires the complete analysis.

Consider first the half-wave axial slot shown in figure 3(a). The electric field distribution is assumed to be of the form

$$E_\phi(a, \phi, z) = \frac{V_o}{a\phi_o} \cos k_o z \qquad \text{(on slot)}$$

$$E_\phi(a, \phi, z) = 0 \qquad \text{(off slot)} \qquad (26)$$

$$E_z(a, \phi, z) = 0 \qquad \text{(everywhere)}$$

From equation (21), the transform of E_ϕ is

$$\bar{E}_{m\phi}(a, k_z) = \frac{1}{(2\pi)^2} \int_{zo/2}^{zo/2} \int_{\phi o/2}^{\phi o/2} \frac{V_o}{a\phi_o} \cos k_o z \, e^{jm\phi} \, e^{jk_o z \cos\theta} \, d\phi dz \qquad (27)$$

---

[1]On the conducting portion of the cylinder, the discontinuity of $\vec{H}$ is equal to the surface currents. On the aperture, $\vec{H}$ is continuous, therefore, the surface $\rho = a$ requires "mixed" boundary conditions.

where the far field substitution $k_z = k_o \cos\theta$ has been made from the discussion in appendix B.

Since $z_o = \frac{\lambda_o}{2} = \frac{\pi}{k_o}$, the integral, when evaluated, becomes

$$\bar{E}_{m\phi} = \frac{1}{2\pi^2} \frac{V_o}{a} \left[\frac{\sin\left(\frac{m\phi_o}{2}\right)}{\left(\frac{m\phi_o}{2}\right)} \right] \frac{\cos\left(\frac{\pi}{2}\cos\theta\right)}{k_o \sin^2\theta} \tag{28}$$

If the slot is sufficiently thin so that $\frac{m\phi_o}{2} << 1$, then $\frac{\sin\left(\frac{m\phi_o}{2}\right)}{\left(\frac{m\phi_o}{2}\right)} \approx 1$,

and the transformed fields at $\rho = a$ are

$$\left.\begin{aligned} \bar{E}_{mz} &= 0 \\ \bar{E}_{m\phi} &= \frac{V_o}{2\pi^2 k_o a} \frac{\cos\left(\frac{\pi}{2}\cos\theta\right)}{\sin^2\theta} \end{aligned}\right\} \tag{29}$$

The substitution of equation (29) into equation (25) gives

$$\left.\begin{aligned} c_m &= -\frac{V_o}{2\pi^2 k_o a} \frac{\cos\left(\frac{\pi}{2}\cos\theta\right)}{\sin^2\theta} \frac{L_{14}}{L_{12} L_{44} - L_{42} L_{14}} \\ d_m &= \frac{V_o}{2\pi^2 k_o a} \frac{\cos\left(\frac{\pi}{2}\cos\theta\right)}{\sin^2\theta} \frac{L_{12}}{L_{12} L_{44} - L_{42} L_{14}} \end{aligned}\right\} \tag{30}$$

From equation (B-15), the Poynting vector is

$$\vec{S} = \frac{1}{2(k_o r)^2 Z_o} \left(\frac{V_o}{a}\right)^2 P_1(\theta, \phi)\, \vec{u}_r \tag{31}$$

Where $P_1(\theta, \phi)$ is the power pattern factor defined by

$$P_1(\theta, \phi) = \omega^2 \frac{\cos^2\left(\frac{\pi}{2}\cos\theta\right)}{\pi^4 \sin^2\theta} \left[Z_o^2 \left| \sum_{m=-\infty}^{\infty} \frac{L_{12}\, e^{-jm(\phi-\pi/2)}}{L_{12} L_{44} - L_{42} L_{14}} \right|^2 + \left| \sum_{m=-\infty}^{\infty} \frac{L_{14}\, e^{-jm(\phi-\pi/2)}}{L_{12} L_{44} - L_{42} L_{14}} \right|^2 \right] \tag{32}$$

It is understood that $L_{ij} = L_{ij}(m, \theta)$. Consider now the half-wave circumferential slot shown in figure 3(b). In this case, the electric field is assumed to have the distribution

$$\left.\begin{aligned} E_z(a, \phi, z) &= \frac{V_o}{z_o}\cos(k_o a\phi) && \text{(on slot)} \\ E_z(a, \phi, z) &= 0 && \text{(off slot)} \\ E_\phi(a, \phi, z) &= 0 && \text{(everywhere)} \end{aligned}\right\} \tag{33}$$

For this polarization, the transformed electric field is

$$\bar{E}_{mz} = \frac{1}{(2\pi)^2}\frac{V_o}{z_o}\int_{-z_o/2}^{z_o/2}\int_{-\phi_o/2}^{\phi_o/2} \cos(k_o a\phi)\, e^{jm\phi}\, e^{jk_o z\cos\theta}\, d\phi dz \tag{34}$$

Because $a\phi_o = \frac{\lambda_o}{2} = \frac{\pi}{k_o}$, the result of integration is

$$\bar{E}_{mz} = \frac{V_o}{2\pi^2}\frac{\sin\left(k_o\frac{z_o}{2}\cos\theta\right)}{\left(k_o\frac{z_o}{2}\cos\theta\right)} k_o a \frac{\cos\left(\frac{m\pi}{2k_o a}\right)}{\left[\left(k_o a\right)^2 - m^2\right]} \tag{35}$$

If the slot is thin, then the specified fields at $\rho = a$ are

$$\bar{E}_{a\phi} = 0$$

$$\bar{E}_{az} = \frac{V_o}{2\pi^2} k_o a \frac{\cos\left(\frac{m\pi}{2k_o a}\right)}{\left[(k_o a)^2 - m^2\right]} \tag{36}$$

Therefore, from equations (25) and (36), the coefficients are

$$c_m = \frac{V_o}{2\pi^2} k_o a \frac{\cos\left(\frac{m\pi}{2k_o a}\right)}{\left[(k_o a)^2 - m^2\right]} \frac{L_{44}}{L_{12} L_{44} - L_{42} L_{14}} \tag{37}$$

$$d_m = -\frac{V_o}{2\pi^2} k_o a \frac{\cos\left(\frac{m\pi}{2k_o a}\right)}{\left[(k_o a)^2 - m^2\right]} \frac{L_{42}}{L_{12} L_{44} - L_{42} L_{14}}$$

From equation (B-15):

$$\vec{S} = \frac{1}{2} \frac{1}{Z_o} \left(\frac{V_o}{r}\right)^2 P_2(\theta,\phi)\, \vec{u}_r \tag{38}$$

where $P_2(\theta,\phi)$ is the pattern factor, defined by:

$$P_2 = \frac{\pi^2}{4} (k_o a)^2 \sin^2\theta \left[\frac{2}{Z_o} \left| \sum_{m=-\infty}^{\infty} \frac{\cos\left(\frac{m\pi}{2k_o a}\right) L_{42}\, e^{-jm(\phi-\pi/2)}}{\left[(k_o a)^2 - m^2\right]\left[L_{12} L_{44} - L_{42} L_{14}\right]} \right|^2 \right. \tag{39}$$

$$\left. + \left| \sum_{m=-\infty}^{\infty} \frac{\cos\left(\frac{m\pi}{2k_o a}\right) L_{44}\, e^{-jm(\phi-\pi/2)}}{\left[(k_o a)^2 - m^2\right]\left[L_{12} L_{44} - L_{42} L_{14}\right]} \right|^2 \right]$$

The index m assumes integer values, consequently, the following relationships hold:

$$\begin{aligned} J_{-m}(x) &= (-1)^m J_m(x) \\ J'_{-m}(x) &= (-1)^m J'_m(x) \\ H^{(2)}_{-m}(x) &= (-1)^m H^{(2)}_m(x) \\ H^{(2)'}_{-m}(x) &= (-1)^m H^{(2)'}_m(x) \end{aligned} \tag{40}$$

As a result of equation (40) the matricies $\left[C^{i+1}_{jk}(-m)\right]$ and $\left[D^1_{jk}(-m)\right]$ expressed in terms of the matrix elements of $\left[C^{i+1}_{jk}(+m)\right]$ and $\left[D^1_{jk}(+m)\right]$ become:

$$\left[C^{i+1}_{jk}(-m)\right] = \begin{bmatrix} C^{i+1}_{11}(m) & C^{i+1}_{12}(m) & -C^{i+1}_{13}(m) & -C^{i+1}_{14}(m) \\ C^{i+1}_{21}(m) & C^{i+1}_{22}(m) & -C^{i+1}_{23}(m) & -C^{i+1}_{24}(m) \\ -C^{i+1}_{31}(m) & -C^{i+1}_{32}(m) & C^{i+1}_{33}(m) & C^{i+1}_{34}(m) \\ -C^{i+1}_{41}(m) & -C^{i+1}_{42}(m) & C^{i+1}_{43}(m) & C^{i+1}_{44}(m) \end{bmatrix} \tag{41}$$

$$\left[D^1_{jk}(-m)\right] = (-1)^m \begin{bmatrix} D^1_{11}(m) & D^1_{12}(m) & -D^1_{13}(m) & -D^1_{14}(m) \\ D^1_{21}(m) & D^1_{22}(m) & -D^1_{23}(m) & -D^1_{24}(m) \\ -D^1_{31}(m) & -D^1_{32}(m) & D^1_{33}(m) & D^1_{34}(m) \\ -D^1_{41}(m) & -D^1_{42}(m) & D^1_{43}(m) & D^1_{44}(m) \end{bmatrix}$$

It can readily be shown that the product of the matrices, $\left[L_{jk}(-m)\right] = \left[D^1_{jk}(-m)\right]\left[C^2_{jk}(-m)\right]\left[C^3_{jk}(-m)\right] \cdots \left[C^{n+1}_{jk}(-m)\right]$ is also in the same form as equation (41)[2]; that is

$$\left[L_{jk}(-m)\right] = (-1)^m \begin{bmatrix} L_{11}(m) & L_{12}(m) & -L_{13}(m) & -L_{14}(m) \\ L_{21}(m) & L_{22}(m) & -L_{23}(m) & -L_{24}(m) \\ -L_{31}(m) & -L_{32}(m) & L_{33}(m) & L_{34}(m) \\ -L_{41}(m) & -L_{42}(m) & L_{43}(m) & L_{44}(m) \end{bmatrix} \tag{42}$$

and, it is of interest to note that for $m = 0$ or $\frac{k_z}{k_o} = \cos\theta = 0$, the matrix (42)[3] becomes

$$\left[L_{jk}\right]_{\substack{m=0 \\ \text{or } k_z=0}} = \begin{bmatrix} L_{11} & L_{12} & 0 & 0 \\ L_{21} & L_{22} & 0 & 0 \\ 0 & 0 & L_{33} & L_{34} \\ 0 & 0 & L_{43} & L_{44} \end{bmatrix} \tag{43}$$

---

[2] A simple method of proving this is to recognize that the C and D matrices, for negative m, can be written in the form $\left[(-1)^{j+k} b_{jk}(m)\right]$, where the element $b_{jk}(m)$ is a 2 by 2 corner matrix (ref. 8). Straightforward matrix multiplication then gives $\left[(-1)^{j+k} b^1_{jk}(m)\right]\left[(-1)^{j+k} b^2_{jk}(m)\right] \cdots \left[(-1)^{j+k} b^N_{jk}(m)\right] = \left[(-1)^{j+k} a_{jk}(m)\right]$, which proves equation (42).

[3] When either $m = 0$ or $k_z = 0$, the C and D matrices are of the form $\begin{bmatrix} b_{11} & 0 \\ 0 & b_{22} \end{bmatrix}$, again the element b_{jk} is a 2 by 2 corner matrix. It can easily be verified that $\begin{bmatrix} b^1_{11} & 0 \\ 0 & b^1_{22} \end{bmatrix}\begin{bmatrix} b^2_{11} & 0 \\ 0 & b^2_{22} \end{bmatrix} \cdots \begin{bmatrix} b^N_{11} & 0 \\ 0 & b^N_{22} \end{bmatrix} = \begin{bmatrix} a_{11} & 0 \\ 0 & a_{22} \end{bmatrix}$, which proves equation (43).

As a consequence of equation (42), the sums appearing in equations (32) and (39) can be converted to sine and cosine series, with the index m assuming integer values between 0 and ∞ to give:

$$P_1(\theta, \phi) = \left[\frac{2\pi \cos\frac{\pi}{2}\cos\theta}{\pi^2 \sin\theta}\right]^2 \left[z_o^2 \left|\sum_{m=0}^{\infty} \frac{j^m L_{12}\cos m\phi}{\left[L_{12}L_{44} - L_{42}L_{14}\right](1+\delta_o^m)}\right|^2 + \left|\sum_{m=1}^{\infty} \frac{j^{m+1} L_{14}\sin m\phi}{L_{12}L_{44} - L_{42}L_{14}}\right|^2\right] \qquad (44)$$

$$P_2(\theta, \phi) = \left[\frac{2\pi k_o a \sin\theta}{\pi^2}\right]^2 \left[z_o^2 \left|\sum_{m=1}^{\infty} \frac{j^{m+1} L_{42}\cos\frac{m\pi}{2k_o a}\sin m\phi}{\left[(k_o a)^2 - m^2\right]\left[L_{12}L_{44} - L_{42}L_{14}\right]}\right|^2 + \left|\sum_{m=0}^{\infty} \frac{j^m L_{44}\cos\frac{m\pi}{2k_o a}\cos m\phi}{(1+\delta_o^m)\left[(k_o a)^2 - m^2\right]\left[L_{12}L_{44} - L_{42}L_{14}\right]}\right|^2\right]$$

δ_o^m is the Kronecker delta and use has been made of the condition that $L_{14} = L_{42} = 0$ for $m = 0$.

For the pattern cuts of interest, the above equations become

(a) In the equatorial plane $(\theta = \pi/2)$:

$$P_1(\pi/2, \phi) = \left(\frac{2\omega Z_o}{\pi^2}\right)^2 \left| \sum_{m=0}^{\infty} \frac{j^m \cos m\phi}{L_{44}(1+\delta_o^m)} \right|^2$$

$$P_2(\pi/2, \phi) = \left(\frac{2\omega k_o a}{\pi^2}\right)^2 \left| \sum_{m=0}^{\infty} \frac{j^m \cos\left(\frac{m\pi}{2k_o a}\right) \cos m\phi}{(1+\delta_o^m)\left[(k_o a)^2 - m^2\right] L_{12}} \right|^2 \qquad (45)$$

where equation (43) has been used.

(b) In the prime meridian plane ($\phi = 0, \pi$)

$$P_1(\theta, {}^{0}_{\pi}) = \left[\frac{2\omega Z_o \cos\left(\frac{\pi}{2}\cos\theta\right)}{\pi^2 \sin\theta}\right]^2 \left| \sum_{m=0}^{\infty} \frac{j^{\pm m} L_{12}}{\left[L_{12} L_{44} - L_{42} L_{14}\right](1+\delta_o^m)} \right|^2$$

$$P_2(\theta, {}^{0}_{\pi}) = \left[\frac{2\omega k_o a \sin\theta}{\pi^2}\right]^2 \left| \sum_{m=0}^{\infty} \frac{j^{\pm m} L_{44} \cos\left(\frac{m\pi}{2k_o a}\right)}{(1+\delta_o^m)\left[(k_o a)^2 - m^2\right]\left[L_{12} L_{44} - L_{42} L_{14}\right]} \right|^2 \qquad (46)$$

where the upper sign on $j^{\pm m}$ is chosen for $\phi = 0$, and the lower sign for $\phi = \pi$.

VII. RESULTS

The purpose of the present effort was to devise a scheme, whereby all the transformed tangential fields at the surface of the conducting cylinder can be directly related to the unknown free-space coefficients, c_m and d_m. This was achieved through a transformation matrix $\left[L_{jk}\right]$, which is computed on an IBM 7094 data processing machine.

The computational procedure is rather involved, and extensive checks are warranted before the scheme can be applied to problems of interest. This will be accomplished by computing radiation patterns (eqs. (45) and (46)) and comparing them with published results and alternate methods. The data presented here will consist entirely of check cases.

Radiation Patterns in the Equatorial Plane

In order to check the L_{44} $(m, k_z = 0)$ matrix element, equatorial patterns of the axial slot were computed from the first of equation (45). Cylinders with circumference-to-wavelength ratios, $k_o a = 2.5$, 8.0, and 12.0 were chosen in order to assess the accuracy of the results as a function of cylinder size.

As an initial test, patterns of uncoated cylinders were computed by the present method, and compared with published work. Silver and Saunders (ref. 9) tabulated patterns strength versus azimuth angle to four decimal places for a cylinder of size $k_o a = 2.5$. Similar data were given to three places by Bailin (ref. 10) for the cylinders

$k_o a = 8.0$ and 12.0. The accuracy depends upon the number of terms retained in the Fourier series which defines the pattern. Silver and Saunders summed to $m = 9$; whereas, Bailin terminated the series at $m \cong 15$ for $k_o a = 8.0$ and $m \cong 23$ for $k_o a = 12.0$. Generally, $2k_o a$ terms are required to achieve 2 percent accuracy. Results are plotted in figure 4. The solid curve represents calculations derived independently from the integration method of reference 5 and the points are the results of the present effort. Comparative data, with more accuracy, are given in table I, where excellent agreement is indicated.

All three cylinders were then coated with a lossy plasma of thickness $k_o (b - a) = 0.1$. No direct check giving the desired accuracy was available in the literature, consequently dual cases were computed from the program developed in reference 5 so that the two procedures could substantiate each other. In the course of the work, an error was discovered in the integration method. This was corrected, and the results for the plasma $\omega/\omega_p = 1$, $\nu/\omega = 0.3$ are plotted in figure 5. As before, the points represent computations by the present method. The results are also listed in table II, where it is indicated that the two schemes differ by at most two in the last decimal place.

Next, the L_{12} $(m, k_z = 0)$ element was checked by computing equatorial patterns of a circumferential slot antenna. The cylinder of size $k_o a = 3.0$ and dielectric thickness $k_o (b - a) = 1.5$ was chosen in order to compare with the published work of Knop (ref. 2). The results for real index of

refraction, n = 1.00, 1.45, and 2.10 are plotted in figure 6. The solid lines were traced directly from Knop's dissertation (ref. 11) and the points were computed from the second of equation (45). Although small deviations occur in the pattern, on-axis ($\phi = 0^\circ$) results (table II) check to four places for n = 1.00 and 1.45, and to three places for n = 2.10.

The axial slot was considered again so that the accuracy could be checked as a function of the imaginary part of up. The results are given in figure 7. For $\omega/\omega_p = 0.8$, the points representing the matrix method do not in any way correspond to the data given by the integration method. (The points in the range $\phi = 40^\circ - 80^\circ$ are off scale.) However, as the ω/ω_p ratio increases toward unity, the agreement becomes much better.

Inspection of the numerical data shows that the build-up of error, surprisingly, is due to error accumulating in the seventh (and perhaps sixth) digit of the computed Bessel functions. Normally, five and six digit accuracy can be accepted; however, as the imaginary part of up increases, $Y_m(up) \rightarrow jJ_m(up)$. Finite differences between the Bessel and Neumann functions occur in the computations; and, for the specific case, $\omega/\omega_p = 0.8$, this difference is preceded by five zeros, and the controlling numbers are therefore inaccurate.

The complex values of up, which correspond to the plasma parameters of figure 7, are given in table IV. Note that the real part of up is positive and the imaginary part is negative. These signs were chosen to assure outgoing, damped traveling waves as $\rho \rightarrow \infty$.

Radiation Patterns in the Prime Meridian Plane

Free-space elevation patterns were computed in order to check the $L_{12}(m, k_z)$ and $L_{44}(m, k_z)$ elements[4] as a function of the axial mode number, $k_z = k_o \cos\theta$. The numerical values of the elements were substituted into equation (46), and patterns were computed for cylinders of size $k_o a = 2.5$, 8.0, and 12.0. Results are given both in figure 8 and table V; again, the points on the graph are those derived from the matrix method.

Patterns for both the axial and circumferential slot are shown for $k_o a = 12.0$; however, only axial slots were considered for the cylinders $k_o a = 2.5$ and 8.0. It is of interest to note that the front lobes of all three axial slot patterns are virtually coincident, and closely approximate the patterns of a slot on a flat ground plane, as noted by Bailin (ref. 10). It should also be pointed out that the series in equation (46) converge much faster as θ decreases from 90° to 0°. This is because the 2 percent accuracy criterion is twice the argument of the Bessel functions, $2k_o a \sin\theta$.

Next, a comparison was made with the work of W. V. T. Rusch (ref. 3). Rusch gave an approximate solution, which assumes that $J_m(ua)$ may be calculated from the leading terms of the Taylor expansion of $J_m(ub)$; that is

$$J_m(ua) \cong J_m(ub) + u(a - b) J_m'(ub)$$

---

[4] $L_{14}(m, k_z) = D_{14}(m, k_z) \equiv 0$ for the uncoated case.

This expansion, of course, assumes that the product

$$u\,(b - a) = \sin^2 \theta - \frac{\omega_p^2}{\omega^2}\,(b - a)$$

is small. At $\theta = 90^\circ$; the product is approximately 0.14 for $\omega/\omega_p = 1.025$ and 0.19 for $\omega/\omega_p = 1.045$. The respective values at $\theta = 30^\circ$ are 0.53 and 0.51. It is expected, therefore, that Rusch's results will be most accurate for θ near 90°. This is evidenced in figure 9. The solid curves were traced directly from reference 3; the points were computed and normalized with respect to Rusch's on-axis value of the $\omega/\omega_p = 1.048$ curve. There is reasonably good agreement for $\theta = 70^\circ$ and $\theta = 90^\circ$; however, the computations for smaller values of θ, indicate that the elevation patterns are somewhat more directional than those given in reference 3. Rusch did not give computations for the rear lobe, consequently, this data given in figure 9 is of academic interest only. Note that the magnitude is less than 10 percent of the main lobe, and that a definite null occurs near $\theta = 60^\circ$.

No other satisfactory comparisons could be made with published results. Although Harris' (ref. 7) formulation for the axial slot appears to be correct, the data seems to be suspect.

Meltz's results (ref. 4) for the circumferential gap antenna were not of sufficient accuracy to fully test the matrix method; nevertheless, computations for three values of θ were made for the cylinder

$k_o a = 32.00$, $k_o (b - a) = 1.40$, $\omega_p/\omega = 0.237$, $\nu/\omega_p = 0.4$. The values of θ chosen were 90°, 20°, and 5°. The imaginary part of ub was well under five for 90° and 20°; however, for $\theta = 5^\circ$, the imaginary part was -7.34, and beyond the range of the computations. The normalization constants for the curves of reference 4 were not given; therefore, only the relative ratio of pattern strength at $\theta = 20^\circ$ to $\theta = 90^\circ$ was meaningful. Comparative ratios did not check with those of reference 4; however, agreement is achieved if the matrix results are squared. Since the matrix method agrees with manual calculations (using Bessel functions given by the computer subroutine), it is suggested that Meltz is plotting power patterns.

As a final check, one mode $\left(m = 1, \frac{k_z}{k_o} = 0.5\right)$ of the L-matrix elements of a coated cylinder was manually computed and compared with the computer results. The calculations agreed to five places. Hence, the method, as applied to one dielectric layer, seems to be limited only by the accuracy of the Bessel functions.

Several Tandem Layers

If any two adjointing layers have equal indices of refraction, or if $n = 1$ for the last layer, the corresponding C-matrix should be a unit matrix. In other words, the boundary is nonexistent. To see if the diagonalization would occur, an air layer was added to all of the one layer cases discussed in the previous sections. Inspection showed that the C-matrix associated with the air layer differed from unity by one part in 10^7 up to the $2k_o$ e azimuthal modes required.

One homogeneous, lossy layer was constructed from three, then six, then twelve layers, each having the same index of refraction. Again, the appropriate C-matrices diagonalized and differed from unity only in the seventh digit.

Two dissimilar dielectrics were considered, and an attempt was made to correlate the results with those obtained from the integration method. Although the integration scheme can account for radial variations in the dielectric constant, sudden discontinuities, or boundaries, are not allowed. Nevertheless, a comparison was desired. This was done by replacing the boundary between the two dielectrics by a more gradual transition, as shown in the inset of figure 10. It can be seen in figure 10 that the patterns derived from both methods are virtually identical. However, the on-axis values differ by 5 percent, which is somewhat larger than expected. Most of the error can be attributed to limitations imposed by the programing of the integration method.

VIII. CONCLUSIONS

Several checks of the matrix method were considered, and the results suggest the following conclusions and recommendations.

1. The method is apparently successful, provided the imaginary part of the product of the radial wave number times a radial dimension is less than five. However, beyond five, significant error accumulates, and is due, in large part, to the limitations of the computer subroutine which calculates Bessel functions of complex arguments. More accurate computations of the Bessel functions will undoubtedly increase the range of the matrix method, and it is strongly recommended that this be done, particularly before interior ($\rho \leq a$) solutions are matched to exterior ones.

2. The multilayered case was considered in order to check the error accumulated when several matrices are multiplied together to give $\left[L_{jk}\right]$. For the computations involving twelve layers, maximum error in $\left[L_{jk}\right]$ was approximately one part in 9×10^6.

3. In the process of checking, it was found that the elevation patterns given by Rusch (ref. 3) are apparently more directional than his approximate results indicate. The check cases also suggest that the elevation patterns given by Meltz (ref. 4) are actually power patterns.

4. It is recommended that the integration method of reference 5 be modified so that multilayered cases can be checked more accurately.

5. It is recommended that a check of the elements associated with tangential $\vec{H}$; that is, L_{22}, L_{24}, L_{32}, and L_{34} be done before interior and exterior solutions are matched. No direct check now exists.

IX. SUMMARY

A slotted-cylinder antenna, coated with concentric layers of conductive dielectric material is developed as a boundary value problem. The formalism follows the procedure as originally outlined by J. R. Wait, except that the boundary conditions are stated in matrix form. The problem is formulated so that the transforms of the four unknown tangential fields E_z, E_ϕ, H_z, and H_ϕ at the aperture are directly related to the two unknown vector potentials A_z and A_z^* through computable products of four-by-four matrices. Further information is then achieved by completing the boundary conditions at the aperture and algebraically solving for all unknowns.

As a means to check the procedure, the radiation fields of half-wave axial and circumferential aperture antennas, with specified electric field distributions, are computed and checked against known results.

X. ACKNOWLEDGMENTS

The author wishes to express his appreciation to his advisor, Dr. T. E. Leinhardt of the Virginia Polytechnic Institute, for his interest and cooperation.

Also, the author would like to thank Mrs. Beverly Latimer of the NASA Analytical Computing Division, for the excellent job of programing the equations.

Finally, the author is indebted to Dr. Henri Hodara and Dr. Charles M. Knop, of the National Engineering Science Company, for many inspiring technical discussions and patience during times of frustration.

XI. REFERENCES

1. Wait, James R.: Electromagnetic Radiation From Cylindrical Structures. Pergamon Press, 1959.

2. Knop, Charles M.: The Radiation Fields From a Circumferential Slot on a Metal Cylinder Coated With a Lossy Dielectric. IRE Trans. on Antennas and Propagation, vol. AP-9, No. 6, Nov. 1961, pp. 535-548.

3. Rusch, W. V. T.: Radiation From a Plasma-Clad Axially Slotted Cylinder. USCEC Rep. 82-201 (AFCRL 714), Univ. of Southern California, May 1962.

4. Meltz, Gerald: Radiation From a Homogeneous Plasma-Covered Slotted Cylinder. Sperry Rand Research Center Rep. RR-64-23, March 1964.

5. Swift, Calvin T.: Radiation From Slotted-Cylinder Antennas in a Reentry Plasma Environment. NASA TN D-2187, Feb. 1964.

6. Friedman, Bernard: Propagation in a Non-Homogeneous Medium. Electromagnetic Waves, Rudolph E. Langer, ed., The Univ. of Wisconsin Press, 1962, pp. 301-309.

7. Harris, J. H.: Radiation Through Cylindrical Plasma Sheaths. Sci. Rep. No. 2 (AFCRL-62-976), Hughes Aircraft Co., Aug. 1962.

8. Hildebrand, F. B.: Methods of Applied Mathematics. Prentice-Hall, Inc., 1958.

9. Silver, Samuel; and Saunders, William K.: The Radiation From a Transverse Rectangular Slot in a Circular Cylinder. J. Appl. Phys, vol. 21, Aug. 1950, pp. 745-749.

10. Beilin, L. L.: The Radiation Field Produced by a Slot in a Large Circular Cylinder. IRE Trans. on Antennas and Propagation, vol. AP-3, No. 3, July 1955, pp. 120-137.

11. Knop, Charles M.: Radiation Characteristics of Apertures in Coated Metal Surfaces. Ph. D. Thesis, Illinois Institute of Technology, 1963.

12. Stratton, J. A.: Electromagnetic Theory. McGraw Hill Book Co., Inc., 1941

XII. VITA

Calvin T. Swift was born February 6, 1937, in Quantico, Virginia. He attended high school in Lynchburg, Virginia, and entered the Massachusetts of Technology in 1955. After receiving the Bachelor of Science Degree in 1959, he was employed as a research engineer with North American Aviation, Inc., in Downey, California. In 1962, he accepted a position at NASA's Langley Research Center, Hampton, Virginia, where his current efforts are directed toward the electromagnetic aspects of reentry.

Mr. Swift is married to the former Joanne Taylor of Bucksport, Maine.

XIII. APPENDIXES

Appendix A: The Electromagnetic Fields and Vector Potentials

All the pertinent information appears in Stratton (ref. 12); however, a review is given for the purpose of completeness.

It is assumed that the stratified medium of figure 1 is free of charges and currents. Consequently, for a harmonic solution of the form $e^{j\omega t}$, the Maxwell equations become

$$\nabla \times \vec{E}^i = -j\omega\mu_o \vec{H}^i \qquad \text{(a)}$$

$$\nabla \times \vec{H}^i = j\omega\epsilon_i \vec{E}^i \qquad \text{(b)} \qquad \text{(A-1)}$$

$$\nabla \cdot \vec{H}^i = 0 \qquad \text{(c)}$$

$$\nabla \cdot \vec{E}^i = 0 \qquad \text{(d)}$$

For fields which are TM (Transverse magnetic) to z; there exists a vector potential, $A_z^i \vec{u}_z$ and a scalar potential, ψ^i defined by:

$$\vec{H}^i = \frac{1}{\mu_o} \nabla \times A_z^i \vec{u}_z \qquad \vec{E}^i = -\nabla\psi^i - j\omega A_z^i \vec{u}_z \qquad \text{(A-2)}$$

where the above expression for $\vec{E}^i$ follows directly from equation (A-1 (a)). If equation (A-2) is substituted into equation (A-1 (b)), then

$$\begin{aligned} j\omega\mu_o \epsilon_i \vec{E}^i &= \nabla \times \nabla \times A_z^i \vec{u}_z = \nabla\left(\nabla \cdot A_z^i \vec{u}_z\right) - \nabla^2 A_z^i \vec{u}_z \\ &= -j\omega\mu_o \epsilon_i \nabla\psi^i + \omega^2 \mu_o \epsilon_i A_z^i \vec{u}_z \end{aligned} \qquad \text{(A-3)}$$

And, when the expression for $\vec{E}^i$ (eq. (A-2) is substituted into equation (A-1d),

$$\nabla^2\psi^i + j\omega\nabla \cdot A_z^i \vec{u_z} = 0 \qquad (A\text{-}4)$$

Equations (A-3) and (A-4) are decoupled by the Lorentz gauge, that is,

$$\nabla \cdot A_z^i \vec{u_z} = - j\omega\mu_o \epsilon^i \psi^i \qquad (A\text{-}5)$$

Giving, for A_z^i;

$$\nabla^2 A_z^i \vec{u_z} + \omega^2\mu_o \epsilon_i A_z \vec{u_z} = 0 \qquad (A\text{-}6)$$

In cylindrical coordinates, equation (A-6) becomes:

$$\frac{1}{\rho}\frac{\partial}{\partial\rho}\left(\rho\frac{\partial A_z^i}{\partial\rho}\right) + \frac{1}{\rho^2}\frac{\partial^2 A_z^i}{\partial\phi^2} + \frac{\partial^2 A_z^i}{\partial z^2} + \omega^2\mu_o \epsilon_i A_z^i = 0 \qquad (A\text{-}7)$$

From the physics of the problem, A_z^i is expressed as an axial Fourier integral and an azimuthal Fourier series, such that:

$$A_z^i(\rho, \phi, z) = \sum_{m=-\infty}^{\infty} e^{-jm\phi} \int_{-\infty}^{\infty} F_m^i(k_z,\rho)\, e^{-jk_z z}\, dk_z \qquad (A\text{-}8)$$

In order to solve equation (A-7), we need only solve the total differential equation:

$$\frac{1}{\rho}\frac{d}{d\rho}\left(\rho\frac{dF_m^i}{d\rho}\right) + \left(\omega^2\mu_o\epsilon_i - k_z^2 - \frac{m^2}{\rho^2}\right)F_m^i = 0 \qquad (A\text{-}9)$$

This is Bessel's equation; and the particular combination of Bessel functions used depends upon the problem.

From equations (A-2), (A-3), and (A-8), the TM fields are:

$$E_\rho^i(\rho, \phi, z) = -\frac{1}{\omega\mu_o \epsilon_i} \sum_{m=-\infty}^{\infty} e^{-jm\phi} \int_{-\infty}^{\infty} k_z \frac{dF_m^i}{d\rho} e^{-jk_z z}\, dk_z$$

$$E_\phi^i(\rho, \phi, z) = -\frac{1}{j\omega\mu_o \epsilon_i \rho} \sum_{m=-\infty}^{\infty} e^{-jm\phi} \int_{-\infty}^{\infty} mk_z F_m^i e^{-jk_z z}\, dk_z$$

$$E_z^i(\rho, \phi, z) = \frac{1}{j\omega\mu_o \epsilon_i} \sum_{m=-\infty}^{\infty} e^{-jm\phi} \int_{-\infty}^{\infty} \left\{ -\frac{1}{\rho}\frac{d}{d\rho}\left(\rho \frac{dF_m^i}{d\rho}\right) + \frac{m^2}{\rho^2} F_m^i \right\} e^{-jk_z z}\, dk_z$$

$$= \frac{1}{j\omega\mu_o \epsilon_i} \sum_{m=-\infty}^{\infty} e^{-jm\phi} \int_{-\infty}^{\infty} u_i^2 F_m^i e^{-jk_z z}\, dk_z \qquad \text{(A-10)}$$

$$H_\rho^i(\rho, \phi, z) = -\frac{j}{\mu_o \rho} \sum_{m=-\infty}^{\infty} e^{-jm\phi} \int_{-\infty}^{\infty} m F_m^i e^{-jk_z z}\, dk_z$$

$$H_\phi^i(\rho, \phi, z) = -\frac{1}{\mu_o} \sum_{m=-\infty}^{\infty} e^{-jm\phi} \int_{-\infty}^{\infty} \frac{dF_m^i}{d\rho} e^{-jk_z z}\, dk_z$$

$$H_z^i(\rho, \phi, z) = 0$$

Since no free charges exist in the media, auxiliary axial potentials may be constructed defining fields TE (Transverse electric) to z: Such that

$$\vec{E}^i = -\frac{1}{\epsilon_i} \nabla \times A_z^{*i} \vec{u}_z \qquad \vec{H}^i = -\nabla V^{*i} - j\omega A_z^{*i} \vec{u}_z \qquad \text{(A-11)}$$

As before, two equations for V^{*i} and A_z^{*i} may be derived which are decoupled by the Lorentz gauge:

$$\nabla \cdot A_z^{*i} \vec{u_z} = - j\omega \mu_o \epsilon_i \psi^{*i} \qquad \text{(A-12)}$$

Therefore, the substitution of equations (A-11) and (A-12) into equation (A-1a) gives:

$$j\omega \mu_o \epsilon_i \vec{H}^i = \nabla \times \nabla \times A_z^{*i} \vec{u_z} = \nabla\left(\nabla \cdot A_z^{*i} \vec{u_z}\right) - \nabla^2 A_z^{*i} \vec{u_z}$$

$$= \nabla\left(\nabla \cdot A_z^{*i} \vec{u_z}\right) + \omega^2 \mu_o \epsilon^i A_z^{*i} \vec{u_z} \qquad \text{(A-13)}$$

Equation (A-13) is the wave equation, the solution of which is:

$$A_z^{*i}(\rho, \phi, z) = \sum_{m=-\infty}^{\infty} e^{-jm\phi} \int_{-\infty}^{\infty} G_m^i(k_z, \rho)\, e^{-jk_z z}\, dk_z \qquad \text{(A-14)}$$

where G_m^i is a linear combination of Bessel functions. From equations (A-11) and (A-13) the TE fields are:

$$E_\rho^i(\rho, \phi, z) = \frac{j}{\rho \epsilon_i} \sum_{m=-\infty}^{\infty} e^{-jm\phi} \int_{-\infty}^{\infty} m\, G_m^i\, e^{-jk_z z}\, dk_z$$

$$E_\phi^i(\rho, \phi, z) = \frac{1}{\epsilon_i} \sum_{m=-\infty}^{\infty} e^{-jm\phi} \int_{-\infty}^{\infty} \frac{dG_m^i}{d\rho}\, e^{-jk_z z}\, dk_z$$

$$E_z^i(\rho, \phi, z) = 0 \qquad \text{(A-15)}$$

$$H_\rho^i(\rho, \phi, z) = - \frac{1}{\omega \mu_o \epsilon_i} \sum_{m=-\infty}^{\infty} e^{-jm\phi} \int_{-\infty}^{\infty} k_z \frac{dG_m^i}{d\rho}\, e^{-jk_z z}\, dk_z$$

$$H_\phi^i(\rho, \phi, z) = - \frac{1}{j\omega \mu_o \epsilon_i \rho} \sum_{m=-\infty}^{\infty} e^{-jm\phi} \int_{-\infty}^{\infty} m\, k_z\, G_m^i\, e^{-jk_z z}\, dk_z$$

$$H_z^i(\rho, \phi, z) = \frac{1}{j\omega\mu_o \epsilon_i} \sum_{m=-\infty}^{\infty} e^{-jm\phi} \int_{-\infty}^{\infty} u_i^2 G_m^i e^{-jk_z z} dk_z \tag{A-15}$$

And the total fields are obtained by superimposing equations (A-10) and (A-15); that is,

$$E_\rho = \sum_{m=-\infty}^{\infty} e^{-jm\phi} \int_{-\infty}^{\infty} dk_z e^{-jk_z z} \left\{ -\frac{k_z}{\omega\mu_o \epsilon_i} \frac{dF_m^i}{d\rho} + \frac{jmG_m^i}{\rho\epsilon_i} \right\}$$

$$E_\phi^i = \sum_{m=-\infty}^{\infty} e^{-jm\phi} \int_{-\infty}^{\infty} dk_z e^{-jk_z z} \left\{ -\frac{k_z m F_m^i}{j\omega\mu_o \epsilon_i \rho} + \frac{1}{\epsilon_i} \frac{dG_m^i}{d\rho} \right\}$$

$$E_z = \sum_{m=-\infty}^{\infty} e^{-jm\phi} \int_{-\infty}^{\infty} dk_z e^{-jk_z z} \left\{ \frac{u_i^2 F_m^i}{j\omega\mu_o \epsilon_i} \right\} \tag{A-16}$$

$$H_\rho^i = \sum_{m=-\infty}^{\infty} e^{-jm\phi} \int_{-\infty}^{\infty} dk_z e^{-jk_z z} \left\{ -\frac{k_z}{\omega\mu_o \epsilon_i} \frac{dG_m^i}{d\rho} - \frac{jmF_m^i}{\mu_o \rho} \right\}$$

$$H_\phi = \sum_{m=-\infty}^{\infty} e^{-jm\phi} \int_{-\infty}^{\infty} dk_z e^{-jk_z z} \left\{ -\frac{k_z m G_m^i}{j\omega\mu_o \epsilon_i \rho} - \frac{1}{\mu_o} \frac{dF_m^i}{d\rho} \right\}$$

$$H_z^i = \sum_{m=-\infty}^{\infty} e^{-jm\phi} \int_{-\infty}^{\infty} dk_z e^{-jk_z z} \left\{ \frac{u_i^2 G_m^i}{j\omega\mu_o \epsilon_i} \right\}$$

Appendix B: The Far Fields

From equations (3) and (4), the vector potentials in the free-space region $(i = n + 1)$ are:

$$A_z^{n+1}(\rho, \phi, z) = \int_{-\infty}^{\infty} \sum_{m=-\infty}^{\infty} c_m(k_z)\, H_m^{(2)}(u_o \rho)\, e^{-jm\phi}\, e^{-jk_z z}\, dk_z \tag{B-1}$$

$$A_z^{*n+1}(\rho, \phi, z) = \int_{-\infty}^{\infty} \sum_{m=-\infty}^{\infty} d_m(k_z)\, H_m^{(2)}(u_o \rho)\, e^{-jm\phi}\, e^{-jk_z z}\, dk_z$$

In order to evaluate the above integrals in the far field, it is convenient to transform to sperical coordinates, $\rho = r \sin\theta$, $z = r \cos\theta$, such that equation (B-1) becomes:

$$A_z^{n+1}(r, \phi, \theta) = \int_{-\infty}^{\infty} \sum_{m=-\infty}^{\infty} c_m(k_z)\, H_m^{(2)}(u_o\, r \sin\theta)\, e^{-jk_z r \cos\theta}\, e^{-jm\phi}\, dk_z \tag{B-2}$$

$$A_z^{*n+1}(r, \phi, \theta) = \int_{-\infty}^{\infty} \sum_{m=-\infty}^{\infty} d_m(k_z)\, H_m^{(2)}(u_o\, r \sin\theta)\, e^{-jk_z r \cos\theta}\, e^{-jm\phi}\, dk_z$$

Then for large r, and for $0 < \theta < \pi$, the asymptotic expansion of the Hankel function can be substituted into equation (B-2) to give:

$$A_z^{n+1}(r, \phi, \theta) = \sum_{m=-\infty}^{\infty} e^{-jm\phi}\, e^{j\pi/4}\, e^{jm\pi/2}\, I_{1m}(r, \theta) \tag{B-3}$$

$$A_z^{*n+1}(r, \phi, \theta) = \sum_{m=-\infty}^{\infty} e^{-jm\phi}\, e^{j\pi/4}\, e^{jm\pi/2}\, I_{2m}(r, \theta)$$

where:

$$I_{1m} = \int_{-\infty}^{\infty} c_m(k_z) \left[\frac{2}{\pi u\, r \sin\theta}\right]^{1/2} e^{-jr\left[u_o \sin\theta + k_z \cos\theta\right]}\, dk_z$$

$$= \int_{-\infty}^{\infty} g_1(k_z)\, e^{jrf(k_z)}\, dk_z$$

$$I_{2m} = \int_{-\infty}^{\infty} d_m(k_z) \left[\frac{2}{\pi u_o\, r \sin\theta}\right]^{1/2} e^{-jr\left[u_o \sin\theta + k_z \cos\theta\right]}\, dk_z \tag{B-4}$$

$$= \int_{-\infty}^{\infty} g_2(k_z)\, e^{jrf(k_z)} dk_z$$

The integrals of equation (B-4) are difficult to evaluate in general; however, for large r, either saddle point or stationary phase methods may be used to achieve an asymptotic solution. From equations (75) - (78) of reference 2, the latter method gives:

$$I \simeq e^{jrf(k_{oz})}\, g(k_{oz}) \sqrt{\frac{2\pi j}{rf''(k_o z)}} + O\left(\frac{1}{r}\right) \tag{B-5}$$

where k_{oz} is found from the stationary phase condition:

$$f(k_{oz})' = \left.\frac{df(k_z)}{dk_z}\right|_{k_z = k_{oz}} = 0 \qquad \text{(B-6)}$$

Applying the above equation gives

$$k_{oz} = k_o \cos\theta \qquad \text{(B-7)}$$

Therefore:

$$f(k_{oz}) = -k_o$$

$$f''(k_{oz}) = \frac{1}{k_o \sin^2\theta} \qquad \text{(B-8)}$$

The axymptotic solutions of the integrals (B-4) are:

$$I_{1m} = 2\,\frac{e^{-jk_o r}}{r}\, e^{j\pi/4}\, c_m(\theta)$$

$$\text{(B-9)}$$

$$I_{2m} = 2\,\frac{e^{-jk_o r}}{r}\, e^{j\pi/4}\, d_m(\theta)$$

And, the potentials are:

$$A_z^{n+1}(r, \phi, \theta) = 2j\,\frac{e^{-jk_o r}}{r} \sum_{m=-\infty}^{\infty} c_m(\theta)\, e^{-jm(\phi-\pi/2)}$$

$$\text{(B-10)}$$

$$A_z^{*n+1}(r, \phi, \theta) = 2j\,\frac{e^{-jk_o r}}{r} \sum_{m=-\infty}^{\infty} d_m(\theta)\, e^{-jm(\phi-\pi/2)}$$

From the relationships $r = \sqrt{\rho^2 + z^2}$, $\rho = r \sin\theta$, $z = r \cos\theta$, and equation (2), the far fields become:

$$
\begin{aligned}
E_{\rho}^{n+1} &= j\omega A_z^{n+1} \sin\theta \cos\theta \\
E_{\phi}^{n+1} &= -j\omega Z_o A_z^{*n+1} \sin\theta \\
E_z^{n+1} &= -j\omega A_z^{n+1} \sin^2\theta \\
H_{\rho}^{n+1} &= j\omega A_z^{*n+1} \sin\theta \cos\theta \\
H_{\phi}^{n+1} &= j \frac{\omega}{Z_o} A_z^{n+1} \sin\theta \\
H_z^{n+1} &= -j\omega A_z^{*n+1} \sin^2\theta
\end{aligned}
\qquad \text{(B-1)}
$$

Where terms of higher order than $\frac{1}{r}$ have been neglected.

In spherical coordinates, the components are:

$$
\begin{aligned}
E_r^{n+1} &= 0 & H_r^{n+1} &= 0 \\
E_{\phi}^{n+1} &= -j\omega Z_o A_z^{*n+1} \sin\theta & H_{\phi}^{n+1} &= j \frac{\omega}{Z_o} A_z^{n+1} \sin\theta \\
E_{\theta}^{n+1} &= j\omega A_z^{n+1} \sin\theta & H_{\theta}^{n+1} &= j\omega A_z^{*n+1} \sin\theta
\end{aligned}
\qquad \text{(B-1)}
$$

The radiation patterns are derived from the real part of the Poynting vector, which is defined as:

$$\vec{S} = 1/2 \operatorname{Re} \vec{E} \times \hat{\vec{H}} \qquad \text{(B-1)}$$

where the inverted circumflex over $\vec{H}$ indicates complex conjugate. Substituting equations (B-12) into equation (B-13) gives:

$$\vec{S} = \frac{1}{2} \mathrm{Re} \left(E_\theta \hat{H}_\phi - E_\phi \hat{H}_\theta \right) \vec{u}_r$$

$$= \frac{1}{2} \omega^2 \sin^2 \theta \left[Z_o \left| A_z^{*n+1} \right|^2 + \frac{1}{Z_o} \left| A_z^{n+1} \right|^2 \right] \vec{u}_r \qquad \text{(B-14)}$$

Subetitution of equation (B-10) into equation (B-14) gives the desired result,

$$\vec{S} = \frac{2\omega^2 \sin^2 \theta}{r^2} \left[Z_o \left| \sum_{m=-\infty}^{\infty} d_m (\theta) \, e^{-jm(\phi - \pi/2)} \right|^2 \right.$$

$$\left. + \frac{1}{Z_o} \left| \sum_{m=-\infty}^{\infty} c_m (\theta) \, e^{-jm(\phi - \pi/2)} \right|^2 \right] \vec{u}_r \qquad \text{(B-15)}$$

TABLE I

NORMALIZED PATTERN FACTOR VERSUS AZIMUTH FOR THE UNCOATED CYLINDERS, $k_o a = 2.5$, 8.0 and 12.0

$N\left(\frac{\pi}{2}, \phi\right)$ / ϕ^o	$k_o a = 2.5$ (ref. 9)	$k_o a = 2.5$ (ref. 5)	$k_o a = 2.5$ (computed)	$k_o a = 8.0$ (ref. 10)	$k_o a = 8.0$ (ref. 5)	$k_o a = 8.0$ (computed)	$k_o a = 12.0$ (ref.10)	$k_o a = 12.0$ (ref. 5)	$k_o a = 12.0$ (computed)
0	1.0000	1.0000	1.0000	1.000	1.000	1.000	1.000	1.000	1.000
10	0.9962	0.9963	0.9962	0.997	0.997	0.997	1.000	1.000	1.000
20	0.9860	0.9861	0.9861	0.993	0.992	0.993	0.997	0.997	0.997
30	0.9722	0.9722	0.9723	0.986	0.986	0.986	0.991	0.991	0.991
40	0.9565	0.9565	0.9565	0.966	0.966	0.966	0.979	0.978	0.979
50	0.9355	0.9355	0.9355	0.944	0.943	0.944	0.959	0.959	0.959
60	0.8997	0.8998	0.8998	0.904	0.904	0.904	0.920	0.920	0.920
70	0.8389	0.8390	0.8389	0.845	0.846	0.845	0.867	0.867	0.867
80	0.7541	0.7541	0.7541	0.779	0.779	0.779	0.789	0.789	0.789
90	0.6669	0.6668	0.6669	0.680	0.680	0.680	0.684	0.684	0.684
95		0.6327	0.6327	0.645	0.645	0.645	0.639	0.640	0.639
100	0.6086	0.6086	0.6086	0.600	0.600	0.600	0.579	0.579	0.579
105		0.5934	0.5934	0.534	0.535	0.534	0.518	0.518	0.518
110	0.5828	0.5828	0.5828	0.479	0.479	0.479	0.477	0.477	0.477
115		0.5704	0.5704	0.453	0.453	0.453	0.411	0.411	0.411
120	0.5496	0.5497	0.5497	0.418	0.419	0.418	0.364	0.364	0.364
125		0.5161	0.5161	0.350	0.350	0.350	0.335	0.335	0.335
130	0.4673	0.4674	0.4674	0.295	0.295	0.295	0.268	0.269	0.268
135		0.4043	0.4043	0.293	0.293	0.293	0.248	0.248	0.248
140	0.3314	0.3314	0.3314	0.282	0.281	0.282	0.228	0.228	0.228
145		0.2578	0.2578	0.215	0.215	0.215	0.160	0.160	0.160
150	0.2012	0.2012	0.2012	0.154	0.154	0.154	0.178	0.178	0.178
155		0.1870	0.1871	0.187	0.187	0.187	0.150	0.150	0.150
160	0.2191	0.2191	0.2191	0.205	0.206	0.205	0.087	0.087	0.087
165		0.2704	0.2704	0.141	0.141	0.141	0.143	0.143	0.143
170	0.3179	0.3179	0.3179	0.048	0.048	0.048	0.093	0.093	0.093
175		0.3500	0.3500	0.133	0.133	0.133	0.061	0.061	0.061
180	0.3612	0.3613	0.3613	0.181	0.181	0.181	0.134	0.134	0.134

TABLE II.- NORMALIZED PATTERN FACTOR VERSUS AZIMUTH FOR THE COATED CYLINDERS

$k_o a = 2.5$, 8.0, AND 12.0 ($\omega/\omega_p = 1$, $\nu/\omega = 0.3$, $k_o (b - a) = 0.1$)

$N\left(\frac{\pi}{2}, \phi\right)$ / ϕ°	$k_o a = 2.5$ (ref. 5)	$k_o a = 2.5$ (computed)	$k_o a = 8.0$ (ref. 5)	$k_o a = 8.0$ (computed)	$k_o a = 12.0$ (ref. 5)	$k_o a = 12.0$ (computed)
0	1.0000	1.0000	1.000	1.000	1.000	1.000
10	0.9908	0.9908	0.990	0.990	0.990	0.990
20	0.9638	0.9638	0.961	0.961	0.961	0.961
30	0.9205	0.9205	0.915	0.915	0.914	0.913
40	0.8637	0.8638	0.853	0.853	0.851	0.850
50	0.7967	0.7968	0.776	0.776	0.774	0.773
60	0.7222	0.7221	0.690	0.690	0.684	0.685
70	0.6416	0.6415	0.596	0.596	0.586	0.586
80	0.5563	0.5563	0.500	0.500	0.483	0.482
90	0.4702	0.4703	0.405	0.405	0.383	0.384
95	0.4294	0.4294	0.360	0.360	0.335	0.336
100	0.3918	0.3918	0.319	0.319	0.291	0.291
105	0.3582	0.3582	0.280	0.280	0.249	0.248
110	0.3290	0.3290	0.241	0.241	0.212	0.210
115	0.3033	0.3034	0.208	0.208	0.179	0.179
120	0.2794	0.2794	0.182	0.181	0.148	0.149
125	0.2553	0.2552	0.155	0.155	0.125	0.125
130	0.2291	0.2290	0.127	0.127	0.103	0.102
135	0.2000	0.1999	0.108	0.108	0.083	0.083
140	0.1683	0.1682	0.097	0.097	0.071	0.071
145	0.1358	0.1358	0.080	0.080	0.054	0.053
150	0.1067	0.1068	0.058	0.058	0.046	0.045
155	0.0879	0.0880	0.053	0.053	0.041	0.041
160	0.0856	0.0855	0.056	0.056	0.025	0.027
165	0.0965	0.0964	0.042	0.042	0.030	0.031
170	0.1109	0.1110	0.017	0.017	0.022	0.021
175	0.1219	0.1220	0.031	0.031	0.011	0.010
180	0.1259	0.1260	0.044	0.044	0.026	0.026
$\pi^2 \sqrt{p_1\left(\frac{\pi}{2}, 0\right)}$	7.4035	7.4035	24.754	24.753	37.309	37.318

TABLE III.- ON AXIS ($\phi = 0$) FIELD STRENGTH FOR THE CIRCUMFERENTIAL SLOT

($k_o a = 3.00$, $k_o (b - a) = 1.5$)

	$\sqrt{P_2\left(\frac{\pi}{2}, 0\right)}$	
n	Reference 2	Computed
1.00	0.32349	0.32348
1.45	.42209	.42207
2.10	.32471	.32458

TABLE IV.- COMPLEX VALUES OF u_p AS A FUNCTION OF ω/ω_p FOR THE AXIALLY SLOTTED CYLINDER

$k_o a = 8.0$, $\nu/\omega = 0.5$, $k_o (b - a) = 0.1$, $(\theta = \pi/2)$

ω/ω_p	u_p
.8	2.531 - j5.780
.85	2.542 - j4.916
.90	2.739 - j4.059
.95	3.078 - j3.249

TABLE V.- NORMALIZED PATTERN FACTOR VERSUS POLAR ANGLE FOR THE UNCOATED CYLINDERS $k_o a = 2.5$, 8.0, AND 12.0

(a) $\phi = 0^\circ$

	Axial Slot						Circumferential Slot	
N / θ°	$k_o a = 2.5$ (ref. 9)*	$k_o a = 2.5$ (computed)	$k_o a = 8.0$ (ref. 10)	$k_o a = 8.0$ (computed)	$k_o a = 12.0$ (ref. 10)	$k_o a = 12.0$ (computed)	$k_o a = 12.0$ (ref. 10)	$k_o a = 12.0$ (computed)
30	0.3779	0.3782	0.411	0.411	0.414	1.010	1.010	1.010
45.1					0.626	0.626	1.004	1.004
45.4			0.627	0.627				
50	0.6934	0.6936						
59.6			0.810	0.810				
60.1					0.817	0.817	1.001	1.001
70	0.9018	0.9024						
90	1.0000	1.0000	1.000	1.000	1.000	1.000	1.000	1.000

(b) $\phi = 180^\circ$

	Axial Slot						Circumferential Slot	
N / θ°	$k_o a = 2.5$ (ref. 9)	$k_o a = 2.5$ (computed)	$k_o a = 8.0$ (ref. 10)	$k_o a = 8.0$ (computed)	$k_o a = 12.0$ (ref. 10)	$k_o a = 12.0$ (computed)	$k_o a = 12.0$ (ref. 10)	$k_o a = 12.0$ (computed)
30	0.1884	0.1888	0.115	0.115	0.091	0.091	0.009	0.009
45.1					0.109	0.109	0.004	0.004
45.4			0.143	0.143				
50	0.2760	0.2764						
59.6			0.163	0.163				
60.1					0.122	0.122	0.003	0.003
70	.3376	0.3384						
90	0.3612	0.3613	0.181	0.181	0.134	0.134	0.002	0.002

*The data in reference 9 was multiplied by $\frac{\cos(\pi/2 \cos\theta)}{\sin\theta}$ to give N.

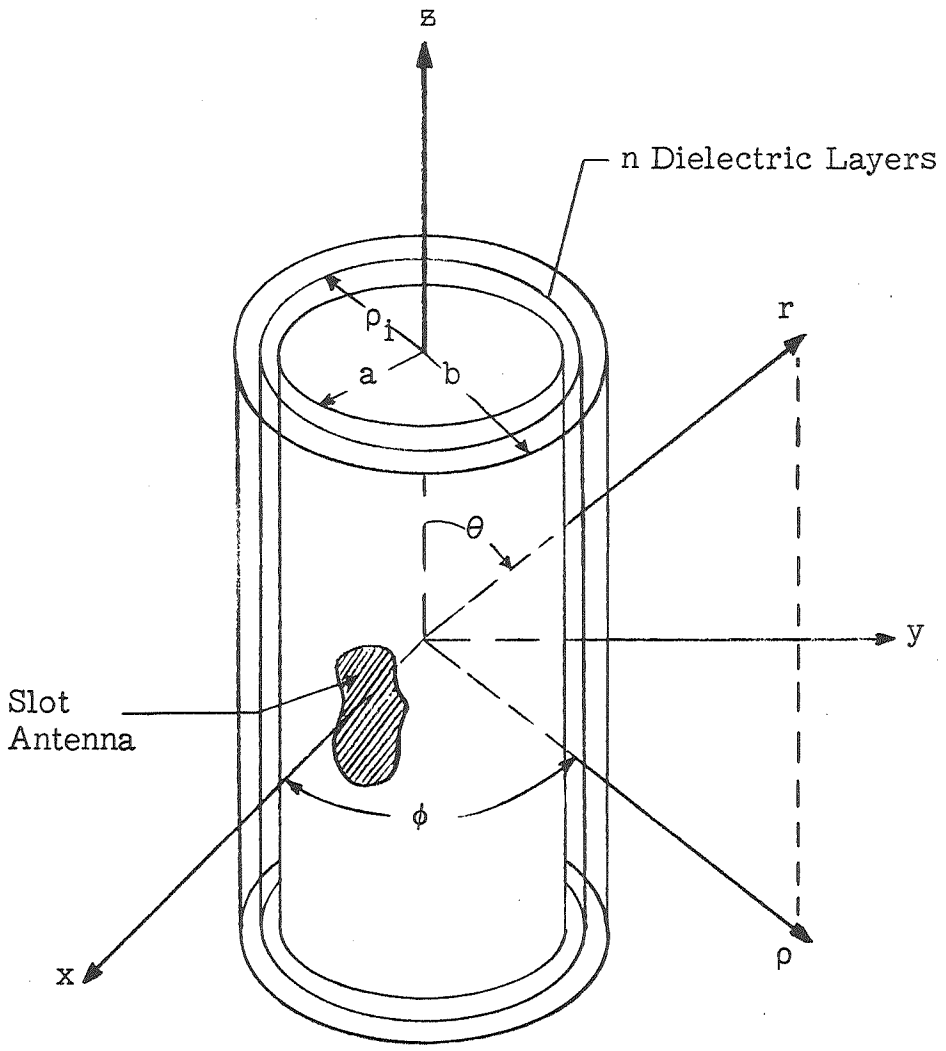

Figure 1.- Geometry of a general slot antenna on a coated, conducting cylinder.

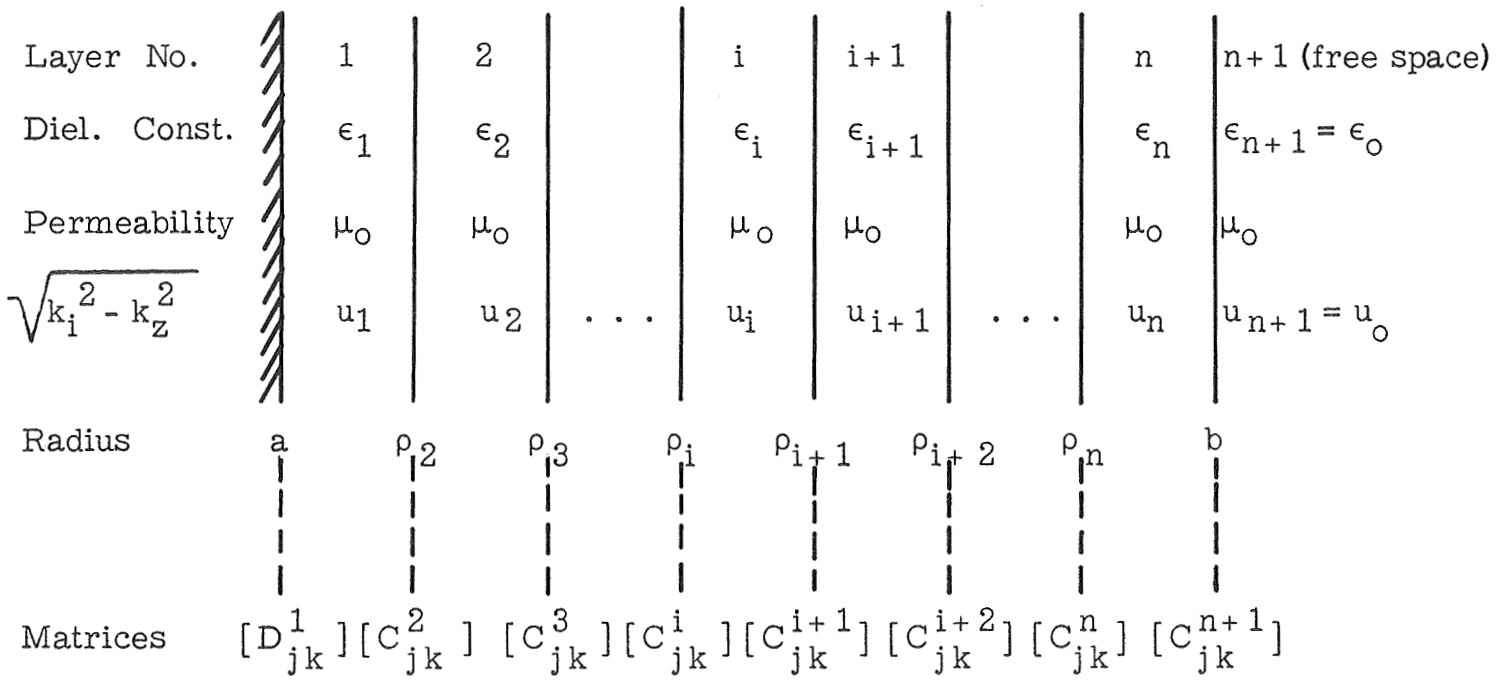

Figure 2.- Schematic for applying boundary conditions.

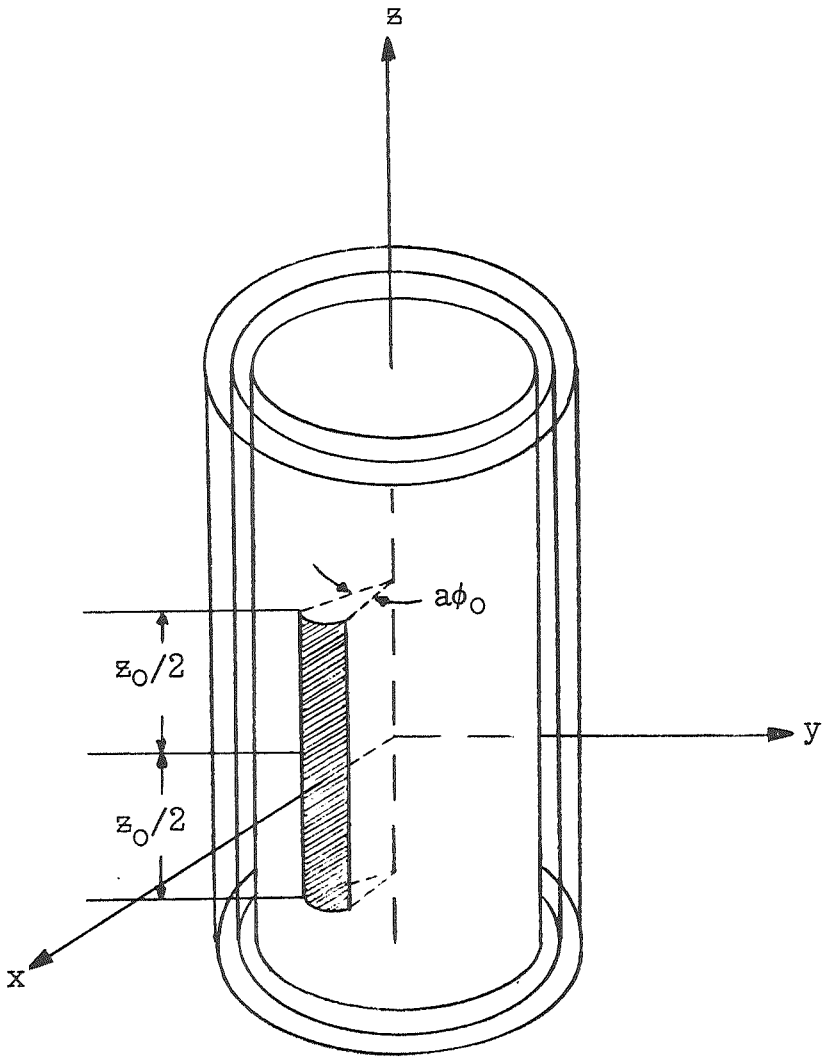

(a) Axial slot.

Figure 3.- Antenna radiating into a stratified medium.

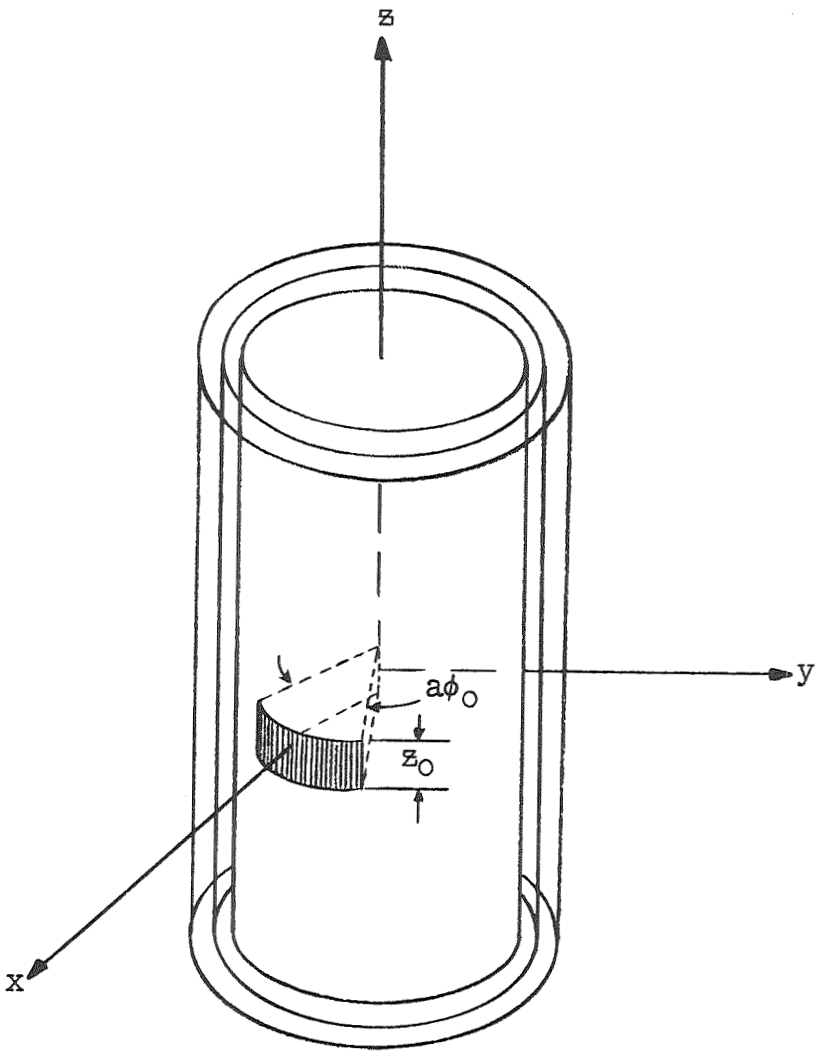

(b) Circumferential slot.

Figure 3 - Concluded.

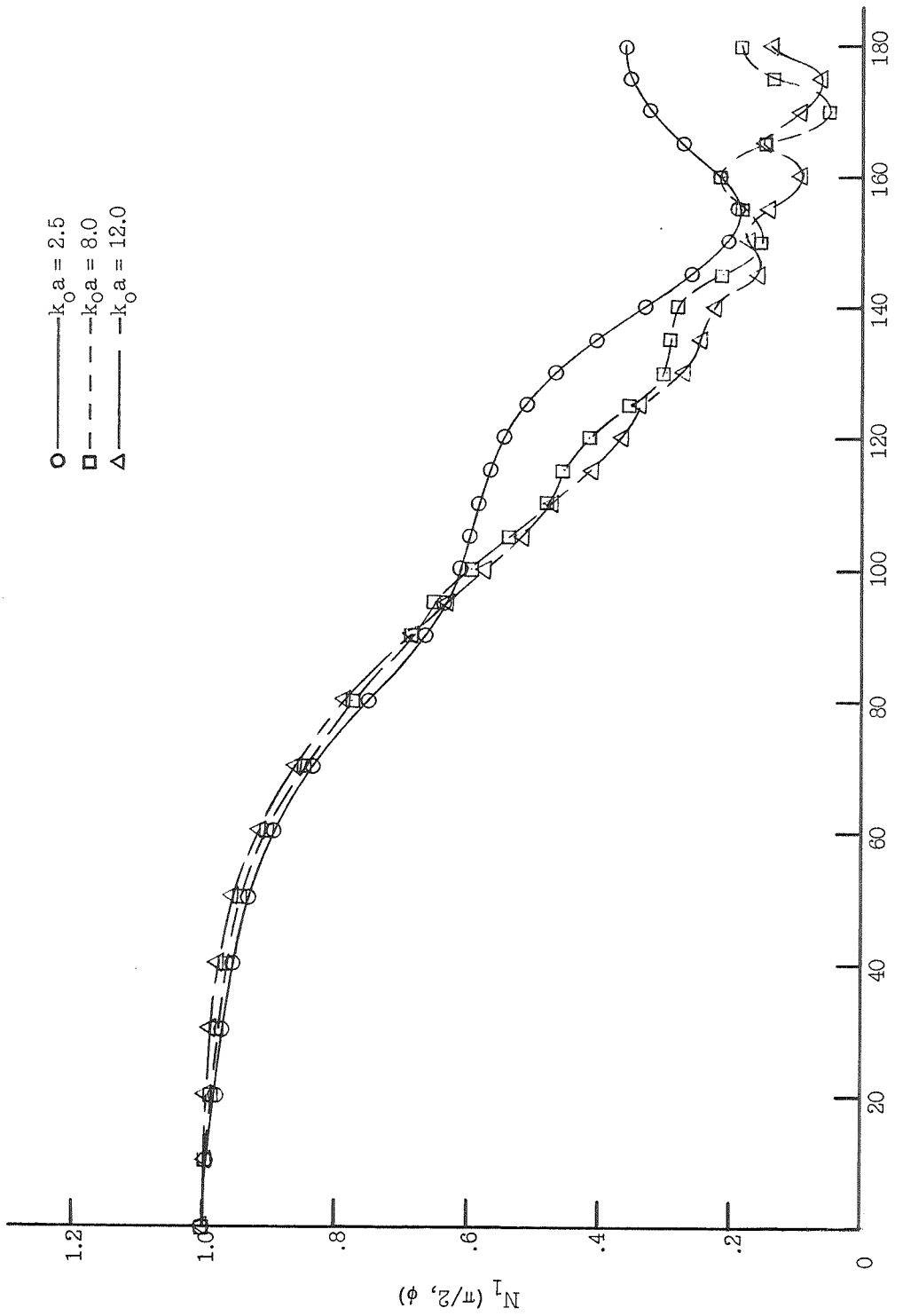

Figure 4.- Equatorial radiation patterns of axially slotted, uncoated cylinders.

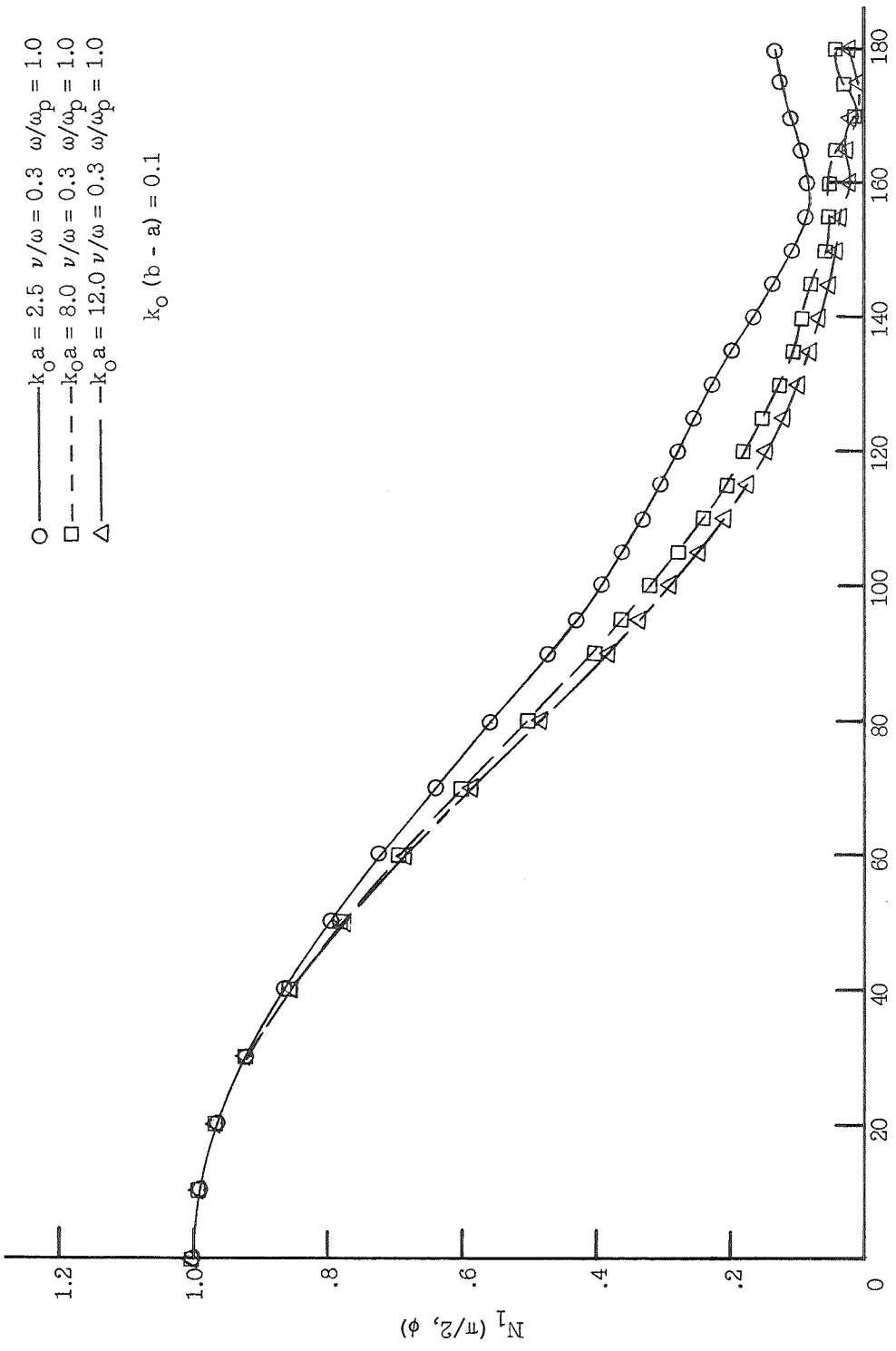

Figure 5.- Equatorial patterns of axially slotted cylinders, coated with a plasma of thickness $k_o (b - a) = 0.1$.

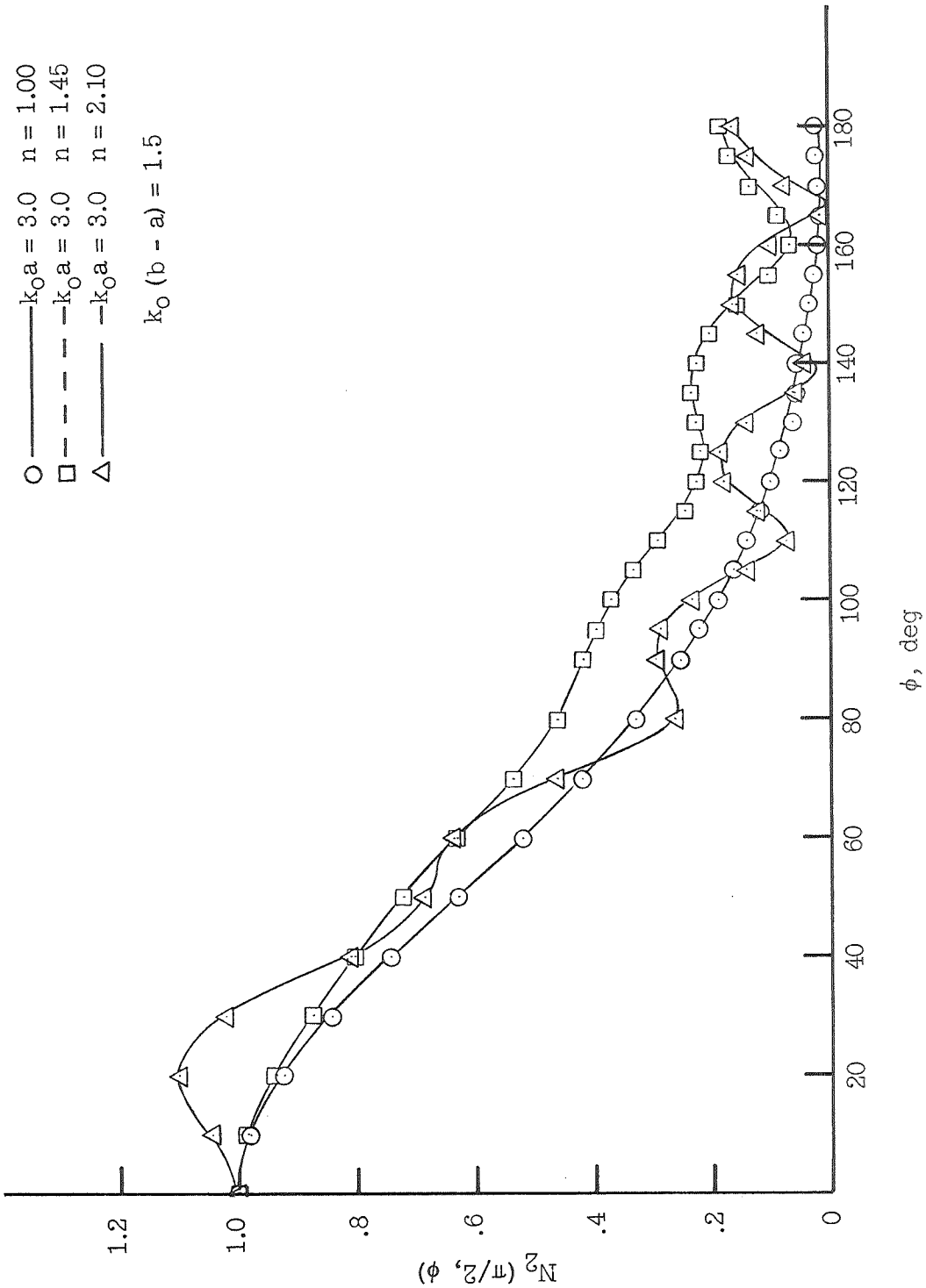

Figure 6.- Equatorial patterns of a circumferentially slotted cylinder, coated with dielectrics of thickness k_o (b - a) = 1.5.

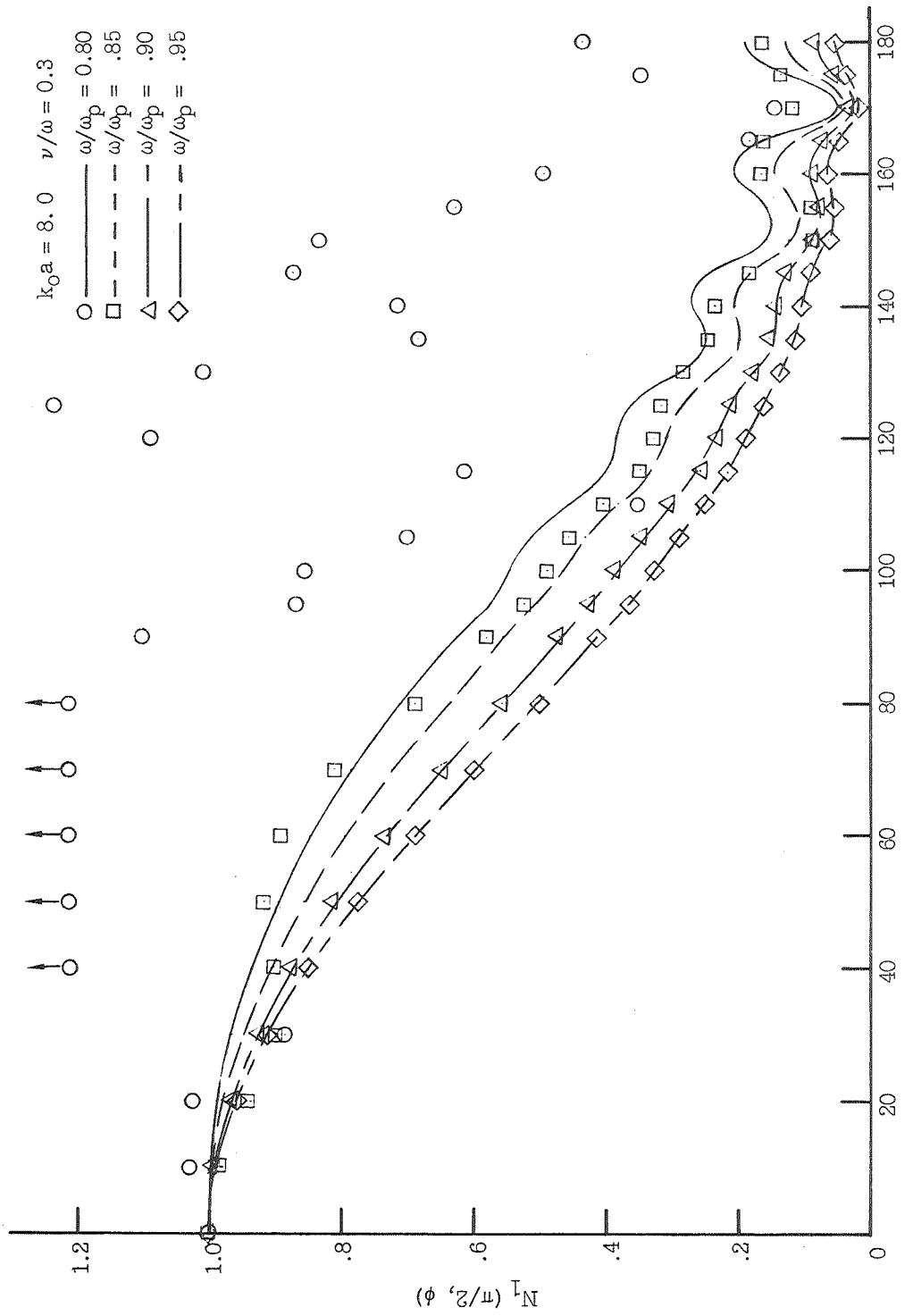

Figure 7.- Equatorial patterns of an axially slotted cylinder, coated with plasmas of thickness k_o (b - a) = 0.1.

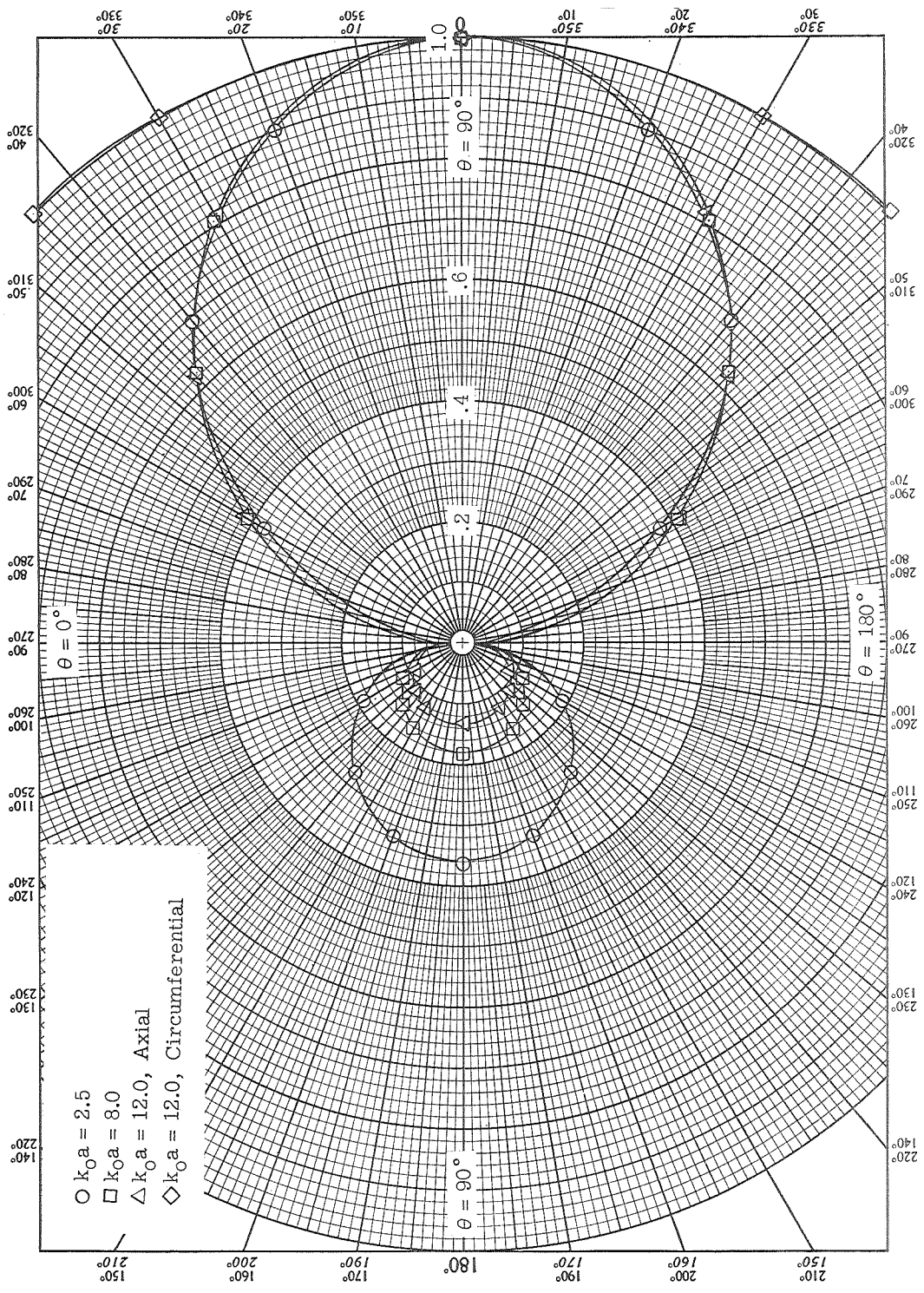

Figure 8. - Elevation patterns of uncoated, slotted cylinders.

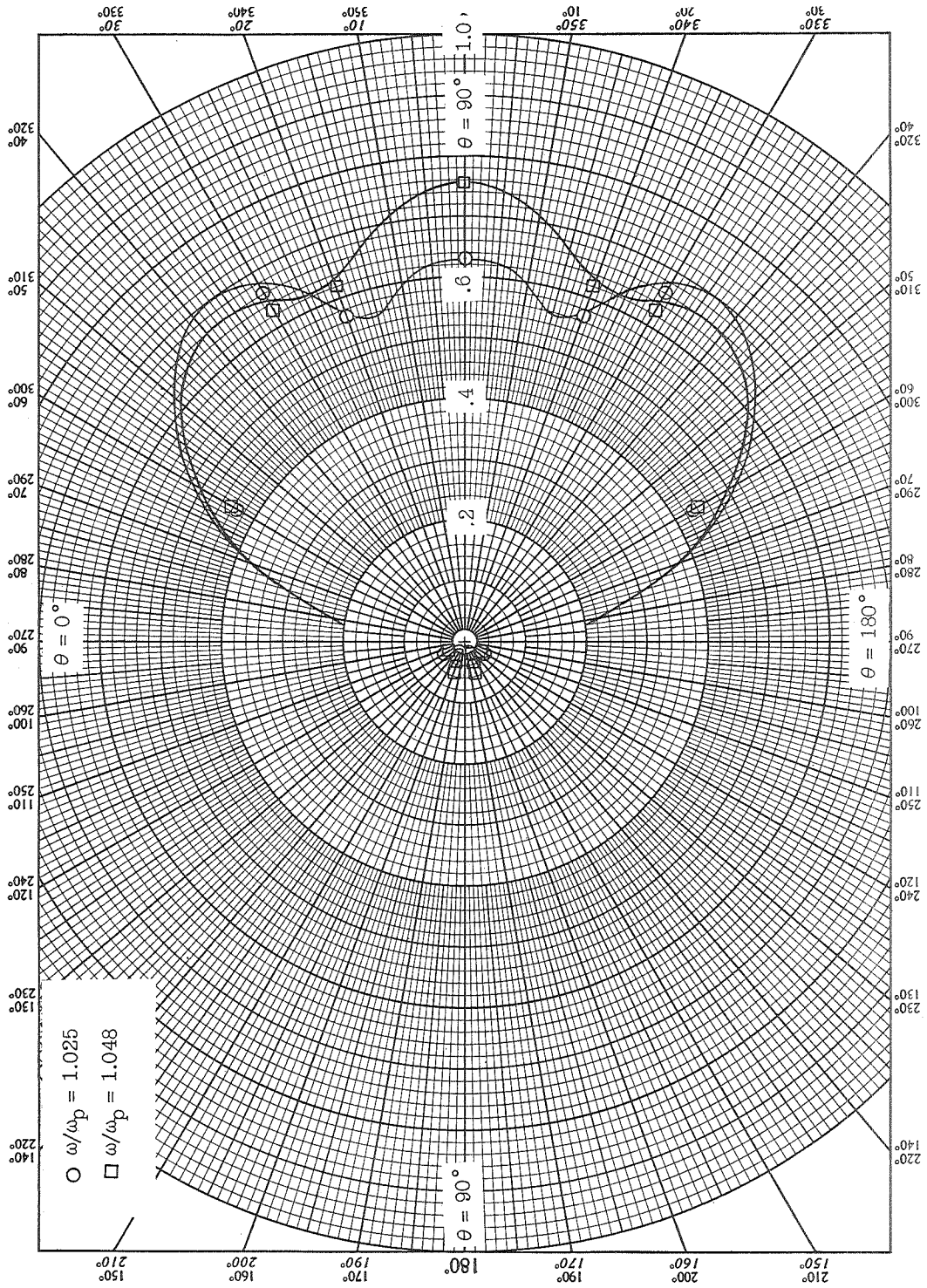

Figure 9.- Elevation patterns of an axially slotted cylinder, coated with a non-lossy plasma.

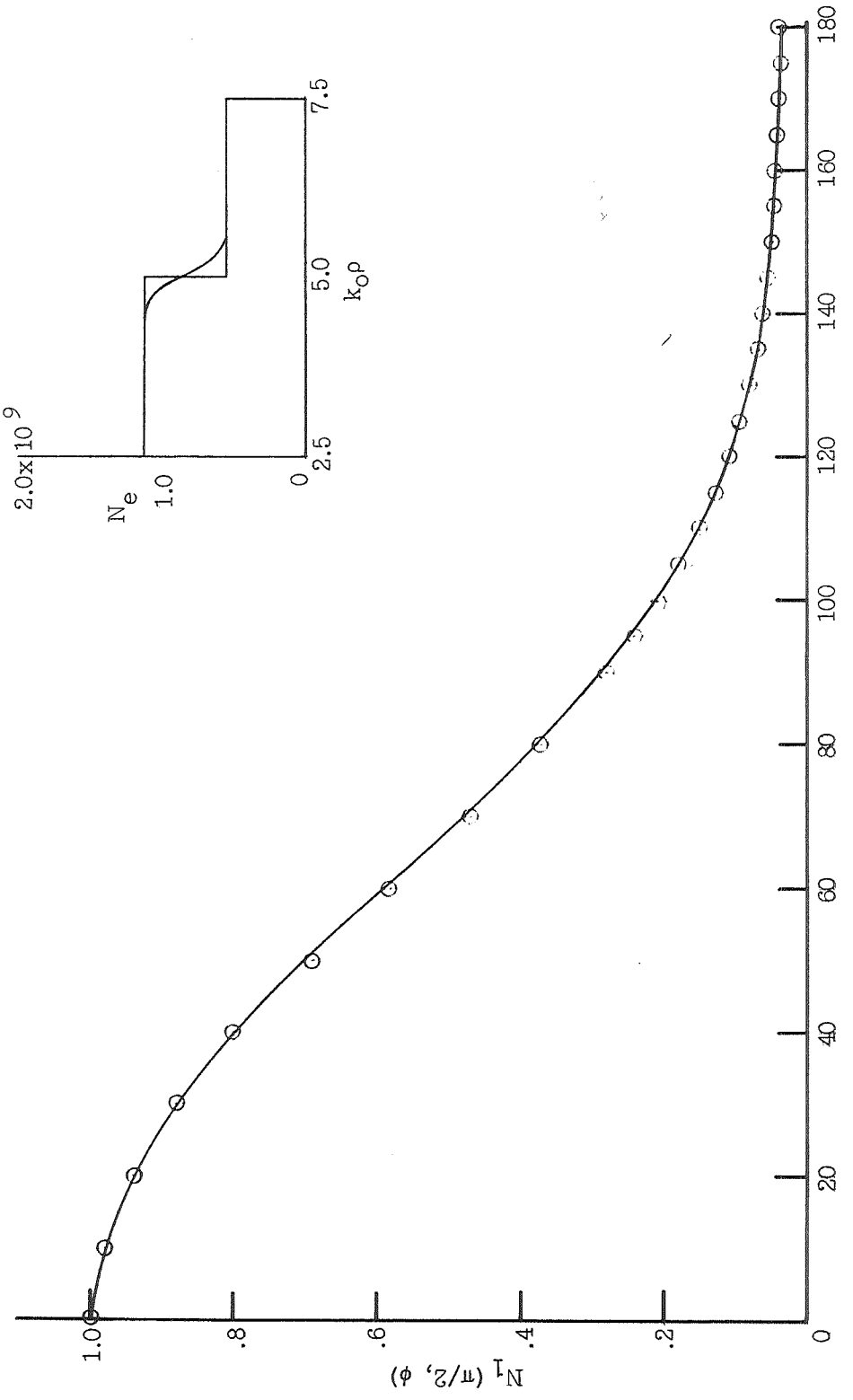

Figure 10.- Radiation pattern of an axially slotted cylinder, coated with two tandem plasma layers.